공학박사학위논문

Selective electrochemical monitoring of poly(alkylene glycol)-based suppressor and halide ion concentration in Cu electrodeposition system using chemical/electrochemical control and artificial neural network

화학적/전기화학적 제어와 인공 신경망을 이용한 구리 전해 도금 시스템에서의 폴리알킬렌글리콜 기반 억제제 및 할로겐화 이온 농도의 선택적 전기화학 모니터링

2021년 8월

서울대학교 대학원

화학생물공학부

윤 영

Selective electrochemical monitoring of poly(alkylene glycol)-based suppressor and halide ion concentration in Cu electrodeposition system using chemical/electrochemical control and artificial neural network

화학적/전기화학적 제어와 인공 신경망을 이용한 구리 전해 도금 시스템에서의 폴리알킬렌글리콜 기반 억제제 및 할로겐화 이온 농도의 선택적 전기화학 모니터링

지도교수 김 재 정

이 논문을 공학박사 학위논문으로 제출함
2021 년 7 월

서울대학교 대학원
화학생물공학부
윤 영

윤영의 공학박사 학위논문을 인준함
2021 년 8 월

위 원 장 _____

부위원장 _____

위 원 _____

위 원 _____

위 원 _____

Abstract

Accurate monitoring of an electroplating bath's chemical balance is a key factor for maintaining its performance during a long-term plating operation. Monitoring the concentration of additives in the copper (Cu) electroplating process is becoming important, but is challenging, because the interaction between additives makes it problematic to observe the independent behavior of a target additive. Monitoring of additives is performed by electrochemical analysis, which provides massive information from the system at once. In the case of chemical species which do not directly participate in the faradaic process of the electrochemical reaction, such as additives in the Cu electrochemical deposition system, it is difficult to obtain quantitative information precisely from the signal in an electrochemical system. Instead, the quantitative information, such as a concentration, of an additive could be determined through the change of the rate of electrochemical reaction involving the metal ion. This approach exhibits the feasibility that quantitative information could be determined even for electrochemically inactive chemical species, but when the Cu electrochemical deposition system contains various types of additives, it becomes challenging to estimate which additive affects the electrochemical signal generated in the analysis since each additive

has a complex effect on the rate of cupric ion (Cu^{2+}) and cuprous ion (Cu^{+}) reduction.

This dissertation covers various methods for electrochemical analyses which increases the selectivity from the concentration of a target additive through chemical and electrochemical control. Iodide ion (I^{-}), an inorganic leveler, has been evaluated as an excellent additive in that it does not produce any byproducts with completely different chemical properties like organic additives. During the operation of plating, I^{-} was consumed via the reaction with Cu^{+} ($Cu^{+} + I \rightarrow CuI$), oxidation reactions ($2I^{-} \rightarrow I_2 + 2e$ and $3I^{-} \rightarrow I_3^{-} + 3e$), as well as a physical incorporation. The I^{-} concentration decrease resulted in a degradation of the bath, while the major byproducts (CuI and I_2) rarely influences on the bath performance for through-silicon via (TSV) filling. In order to monitor the I^{-} concentration by cyclic voltammetry stripping (CVS) analysis, the electrochemical response of I^{-} was examined at various conditions. I^{-} suppressed the Cu electrodeposition rate; this response was dependent on the mass transport of I^{-} and the applied potential of the working electrode. A subsequent effective coverage analysis revealed that not only I^{-} but also copper iodide (CuI) was a key inhibitor, demonstrating that the inhibition of I^{-} becomes weaker at a negative potential. With a responsive curve (RC)-CVS analysis conducted at an optimized condition, a linear relationship between

the real and measured concentrations could be found, irrespective of other additives' concentrations. The method suggested in this dissertation enabled the direct monitoring of the I^- concentration in a Cu plating bath.

Bis-(sulfopropyl)-disulfide (SPS) is a representative accelerator used in Cu electrodeposition and interferes with the inhibition of poly(alkylene) glycol (PAG). Therefore, the presence of SPS causes a problem of lowering the signal-to-noise (SNR) in PAG concentration measurement. In order to disrupt the anti-suppression action of SPS accelerator to monitor the concentrations of PAG suppressor, I^- was introduced as a chemical pretreatment agent, based on its inhibiting action to accelerator in a vigorous mass-transport environment. Even a small amount of SPS in target solutions interfered with the determination of PAG concentration, when using the CVS method as a monitoring tool. I^- could hinder the SPS-mediated breakdown of the surface passivation layer, even in higher concentration of SPS, allowing selective determination of PAG, free from interference by SPS. This is presumed to be due to the formation of the ionic compound, CuI with I^--involved PAG complex on the electrode surface. By introducing I^-, modified CVS analysis was repeated, and the results revealed that adding I^- totally suppressed the behavior of SPS, and yielded determined PAG concentrations that were

similar to the actual values.

Machine learning allows a computer to learn from data by itself, enabling a system to respond based on numerous data and computing power. The superiority of machine learning comes from the building a model based on the data and facilitating the solution itself to adapt to a change raised in the system. When combining the superiority of electrochemical analysis with machine learning, it seems possible to make a model which could extract quantitative information by learning electrochemical data on system variables. Chloride ion (Cl^-) adsorbs on the substrate during the Cu electrodeposition and acts as a traction to induce strong adsorption of polyethylene glycol (PEG), inhibiting the physical access of Cu^{2+} to the substrate. This PEG-Cl^- inhibition layer increases the energy required for Cu^{2+}/Cu^+ reduction and slows down the rate of Cu electrochemical deposition, and it is very challenging to determine each concentration selectively due to the complementary effects of the two additives. In the system composed of PEG3350 and Cl^-, it was possible to easily predict the concentration through data collected in a simple electrochemical analysis and artificial neural network (ANN) model due to the excellent analytical responses of PEG3350 and Cl^- in cyclic voltammetry (CV) analysis. However, in the Cu electrodeposition system containing

PEG of various molecular weights (MWs, PEG200, PEG1500, and PEG3350) and Cl^-, the predictive performance of concentration was poor when the same electrochemical analysis and model were applied, because of the competition in adsorption between PEGs with a limited number of Cl^- in the situation where Cl^- acted as an adsorption point for PEG on the electrode surface. In particular, PEG200, due to the small MW, rarely affect Cu electrodeposition, degrading the performance of concentration prediction. In order to control the effect on the adsorption of PEG in CV analysis, the vertex potential of the CV analysis was converted from –0.4 V to –0.2 V (potential with respect to Ag/AgCl reference electrode), and the analytical response of PEG200 was remarkably increased through I^- pretreatment. The introduction of I^- made various Cu and I-related electrochemical reaction systems, such as reduction of Cu^{2+} to Cu^+ and oxidation of CuI formed in the process, in addition to copper electrodeposition, and PEG showed different effects by MW on this complex reaction. As a result, by shifting the vertex potential in CV and introducing I^- as a secondary halide ion, the signal-to-noise ratio of each PEG and Cl^- was enhanced and the performance of ANN model for predicting each additive concentration improved.

Keywords: Cu electrodeposition, additive, selective monitoring, electrochemical analysis, machine learning

Student number: 2016-21041

Content

List of Figures

CHAPTER I

Introduction

1.1. Cu electrodeposition

Copper (Cu) electrodeposition has been widely used in industrial fields, from fabricating Cu foil to filling Cu interconnect. Cu foil is utilized as a seed layer for further deposition in a form of a copper clad laminate (CCL) on printed circuit board (PCB) and for a current collector in lithium-ion battery, while Cu interconnect transfers electrical signal and power between devices in PCB and integrated circuits (ICs) on a silicon (Si) wafer in a form of trench and via. Recently, as the integration of transistors in a Si-based chip approaches to the limit of process refinement and the demand for high-performance PCB increases, a multi-layered device has been intensively introduced as a form of stacked chips and boards in the vertical direction in order to shorten the length of the interconnection between the devices. Multi-layer board (MLB) and high bandwidth memory (HBM) utilize a vertical micro-scaled via in joining interconnect to interconnect or device to device in a multi-layered substrate. Microvia[1] and through-silicon via (TSV)[2, 3] are key technologies for fabricating the vertical interconnect. These three-

dimensional board and device stacks allow densified ICs, the improvement of signal transfer, and lower power consumption compared to conventional wire bonding, emphasizing the importance for the microvia and TSV technology.

Cu electrodeposition which has been regarded as a key process to fabricate Cu foil with superior property and fill defect-free interconnect in sub-micro and micro-scaled circuits is achieved through an electrochemical reduction of cupric ion (Cu^{2+}). The electrochemical system for Cu electrodeposition is made of two electrodes consisting of a cathode and an anode, or three electrodes with a reference electrode included thereto, and the copper ions (Cu^{2+} and Cu^{+}) in the electrolyte are reduced to Cu metal at the working electrode by applying external electrical power. As the working electrode, Ti drum for Cu foil or patterned wafer and PCB (Figure 1.1) could be used in manufacturing Cu products. When a current or a potential is applied through an external electrical power source, the energy of the electrons in the working electrode becomes higher than the lowest unoccupied molecular orbital (LUMO) energy level of the copper ions in the electrolyte, and thus, charge (electron) transfer occurs in which the electrons of the working electrode spontaneously move to the copper ions, leading to the reduction of the copper ions to Cu metal. The net reaction for the electrochemical reduction of Cu^{2+} consists of two steps: the reduction of Cu^{2+} to cuprous ion (Cu^{+}), the slower step

requiring thermodynamically higher energy, and the reduction of Cu^{+} to Cu, the faster step, and the reaction rates are explained by the unstable characteristics of Cu^{+} in the aqueous solution (Figure 1.2). In addition to the charge transfer reaction, the electrochemical reaction is also restricted by mass transfer of the electroactive species from the bulk electrolyte to the electrode due to the consumption of the copper ions on the surface. The electrolyte is an aqueous type, in general, and includes a source for copper ions and a supporting electrolyte. In addition to the metal source and the supporting electrolyte, various organic and inorganic additives are used in the Cu electroplating solution to control the properties and morphologies of the deposit. Therefore, engineers could control the applied current or potential, mass transfer mode of the electroactive species, and chemical composition of the electrolyte affecting the charge transfer reaction, and through this, it is possible to fabricate Cu products with a desired morphology and physical properties. The scheme of the overall Cu electrodeposition is summarized in Figure 1.2.

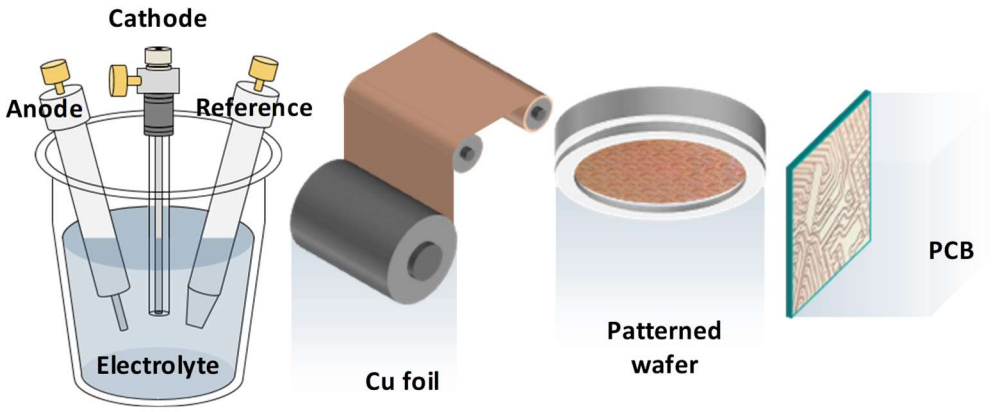

Figure 1.1. Electrochemical system for Cu electrodeposition and various types of cathodes used in industrial field.

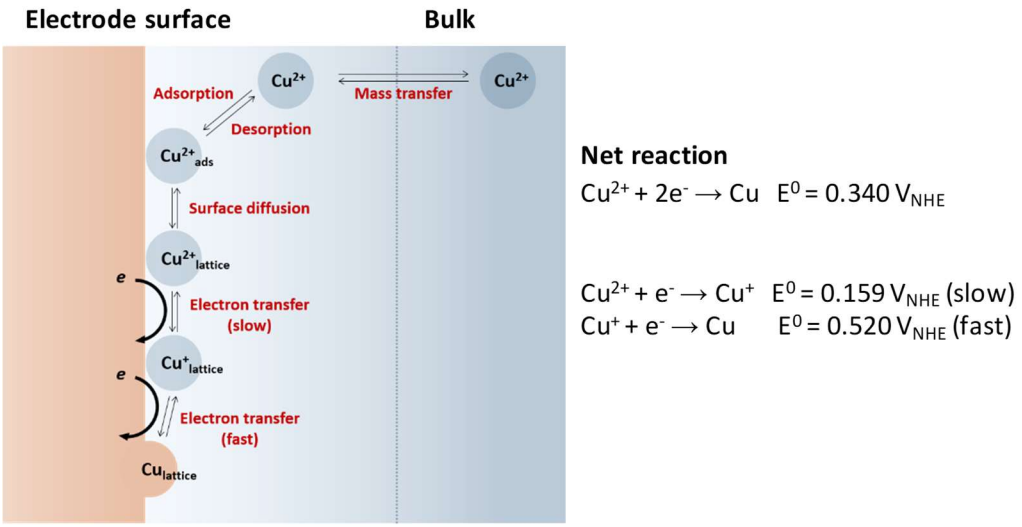

Figure 1.2. Scheme of electrochemical reduction of Cu^{2+} to Cu in Cu electrodeposition process and related standard electrode reactions.

1.2. Process variables of Cu electrodeposition

1.2.1. Applied potential and current

The first controllable variable available to engineers in Cu electrodeposition is applied electrical power to the Cu electrodeposition system. Chronoamperometry, where Cu electrodeposition is performed by applying a constant potential, has the advantages of being able to control the kinetic behavior of Cu^{2+}/Cu^{+} reduction and additives. Particularly, research on the filling high-aspect ratio (HAR) TSV at a constant applied potential using the additive-driven S-shaped negative differential resistance (S-NDR) assisted by the resistive losses of the electrolyte and positive feedback observed in the suppressor-halide Cu electrodeposition system has been attracting attention.[4, 5] Since this approach provides a general framework and optimization roadmap for TSV filling, it enables TSV filling in a single suppressor system even using other metals such as Zn,[6] Ni,[7, 8] Co,[9] and Au.[10] The unique TSV filling profile also supports the passive/active bi-stable steady-state formed in the TSV feature under the co-diffusion of metal ions and suppressors in potentiostatic environments, as simulated in previous study.[11] The chronopotentiometry, a method of applying a constant current, is an approach commonly used in industry, exhibiting an advantage in accurate control of the amount of the deposit.

The convection-dependent behavior of an additive, which would be described later, causes the difference in the overpotential required for Cu electrodeposition depending on the fluidic motion at a constant current. In TSV[12-14] and microvia[15-17] filling, the levelers are selectively adsorbed on the Cu surface near the opening of the feature (i.e., where the electrolyte convection is the strongest), effectively inhibiting Cu growth. As a result, the rate of Cu electrodeposition becomes relatively fast at the bottom of the features where the fluidic motion is weak.

A more advanced method is to apply various forms of potential or current as a function of time. In electrochemical analysis, a potential ramp is applied and current information at various applied potentials is obtained when using linear sweep voltammetry (LSV) and cyclic voltammetry (CV). In Cu electrodeposition, many studies have been conducted to fill features by using a pulse-form potential and current.[18, 19] Figure 1.3(a) describes the application of pulse-reverse electrodeposition for Cu trench filling. Superconformal filling in the accelerator-suppressor system, in general, results from the competitive interaction of the two organic additives and the changes in their adsorption surface coverage. In the pulse-reverse electrodeposition, reverse pulse, or anodic step, could modify the adsorption state between the additives, and thereby could be utilized to improve the filling performance. According to the previous research, the anodic pulse

promotes the displacement of polyethylene glycol (PEG)-Cl^- by bis-(sulfopropyl)-disulfide (SPS) and intensifies additional adsorption of SPS, resulting in changes of the leveling of the filling.[18] Although the shortened incubation time of superfilling could be obtained from the promoted displacement, efficient leveling also could be originated from the deactivation of the accumulated SPS by the anodic step, according to the SPS surface coverage-dependent effect of the anodic step. Therefore, through careful optimization, improving the superfilling performance compared to the constant potential deposition was available.[19]

1.2.2. Transport of electroactive/inactive species

Basically, as the electroactive species, Cu^{2+} and Cu^{+}, are reduced to Cu metal, the concentrations of Cu^{2+}/Cu^{+} at the electrode surface decrease, thereby forming a concentration gradient due to the difference in the concentration with the bulk electrolyte. When the electrochemical reaction occurs, diffusion due to this concentration gradient is inevitably accompanied, and in the absence of external convective conditions, the slower process among the charge transfer reaction and the diffusion of the electroactive species determines the rate of the entire electrochemical reaction. Depending on which

process determines the rate of the electrochemical reaction, the physical properties and morphology of the deposit become different. The Cu electrodeposition in foil and interconnect fabrication prefers charge transfer-controlled Cu^{2+} reduction because it favors a flat surface due to the following chemical/mechanical polishing (CMP) or post-cleaning process. Therefore, the electrodeposition is carried out under low overpotential and current. This condition makes the concentration of Cu^{2+} on the electrode surface sufficient, so that the rate of the reaction is not determined by mass transfer of Cu^{2+}. However, in HAR TSV or microvia filling, the copper ions inside the via is depleted, and therefore an external convective force is required to facilitate mass transfer of the copper ions into the bottom of the via, as in Figure 1.3(b).[20] If the fluidic motion toward the substrate is strengthened using an rotating disk electrode (RDE)-type electrode or a pump, the mass transport of Cu^{2+} into the bottom of the via becomes accessible, so that electroplating is not restricted by mass transfer of Cu^{2+}.

1.2.3. Additives for Cu electrodeposition

The reduction of Cu^{2+} takes place through two steps, the slower process in which Cu^{2+} is reduced to Cu^{+} and the faster step of Cu^{+} reduction to Cu, and the electrochemical

reaction where the unstable Cu^{+} is generated is a rate determining step. The additive changes the rate of Cu electrodeposition by adsorbing on the electrode surface or involving in the electrochemical reduction of copper ions, thereby affecting the morphology and crystal structure of the electrodeposited Cu (Figure 1.3(c)).[21] The additives are combined to obtain the desirable properties of the copper foil or induce bottom-up filling by controlling local rate of electroplating in fabricating Cu via and interconnect. Those additives are classified into the three categories, based on their effect on the rate of Cu electroplating (Figure 1.4).[22] Suppressors such as PEG,[23-27] polypropylene glycol (PPG), and their block copolymer (PEG-PPG-PEG),[28-31] adsorbing faster than accelerators, block the access of Cu^{2+} to the Cu surface by forming a suppressor-chloride (Cl^{-}) blocking layer on the surface.[24, 32, 33] Accelerators such as SPS[34-36] and 3-mercapto-1-propane sulfonate (MPS)[37, 38] displace the pre-adsorbed suppressors and increase the rate of Cu electrodeposition on which they adsorb. Frequently, a combination of SPS, one of poly(alkylene) glycol (PAG) suppressors, and Cl^{-} has been widely adopted and explored in research fields,[39-43] and submicrometer trenches with aspect ratios of 2-6 were filled without defect using the accelerator and suppressor combinations. Levelers, in general, have been used with Cu electrodeposition to remove the topographic variations that occur on the grooved surface, and have also

been adopted to prevent the formation of Cu bumps after Cu superfilling of damascene features.[22, 44, 45] Recently, the levelers have become essential in electrodeposition processes, to achieve defect-free Cu filling of micro-scaled features such as TSVs,[12-14, 46-50] microvias,[16, 17, 51-55] and through-holes (THs).[56-58] Levelers make Cu deposition at the bottom of TSVs and microvias more favorable than at the top and sidewall of the features, resulting in Cu bottom-up filling. To fill THs with defect-free Cu, Cu electrodeposition is selectively promoted in the middle of the THs, a method called butterfly filling, because the Cu filling profiles resemble butterfly wings. These filling processes result from the behavior of the levelers, and considerable research has been conducted to develop better levelers to enhance the Cu filling process.[12-14, 17, 44, 48, 53-59] Commercial levelers like Janus Green B (JGB)[60] and polyvinylpyrrolidones (PVPs) [61, 62] have been additionally used to completely passivate the Cu reduction at the top and side wall of the vias, forming a complex with accelerators, deactivating them, as well as preventing the feature from excess electrodeposition. The adsorption of levelers can be controlled by the convection of electrolytes. Forced convection can promote the adsorption of levelers on the Cu surface by increasing the transfer of levelers to the surface.[12-14, 16, 17, 57] As a result, under stronger convection conditions a Cu surface is

more effectively passivated with a larger number of levelers, compared with weaker convection, which remains relatively poorly passivated. Recently, inorganic species, iodide ion (I^-)[12] and bromide ion (Br^-)[46] have been attracting attention, due to their mass transport-dependent property in TSV filling. It has been shown that the addition of I^- formed copper iodide (CuI) layer on the top of the TSV, which inhibited the growth of Cu at the top, and enabled superfilling. However, the formation of CuI requires one electron and the CuI continuously detached to the bulk solution, resulting in the decrease in filling efficiency. Although Br^- ion showed weaker inhibition effect than I^-, Br^- established stable polymeric suppression layer with PEG-PPG-PEG (EPE suppressor, enhancing the filling efficiency and showing superfilling.

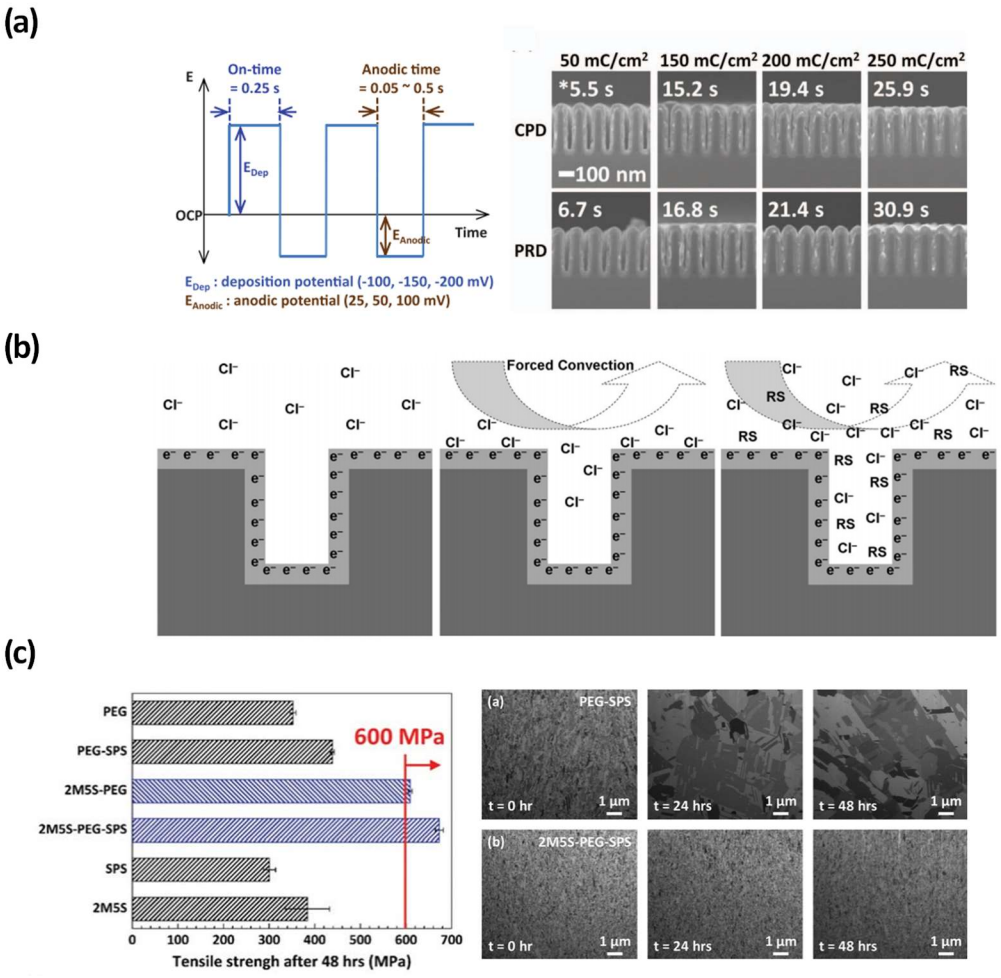

Figure 1.3. (a) Pulse-reverse Cu electrodeposition for gap filling, (ref. 19) (b) convection-dependent adsorption behavior of additives for microvia filling, (ref. 20) and (c) high strength Cu foil prepared by 2-mercapto-5-benzimidazole sulfonic acid (2M5S)-PEG-SPS. (ref. 21)

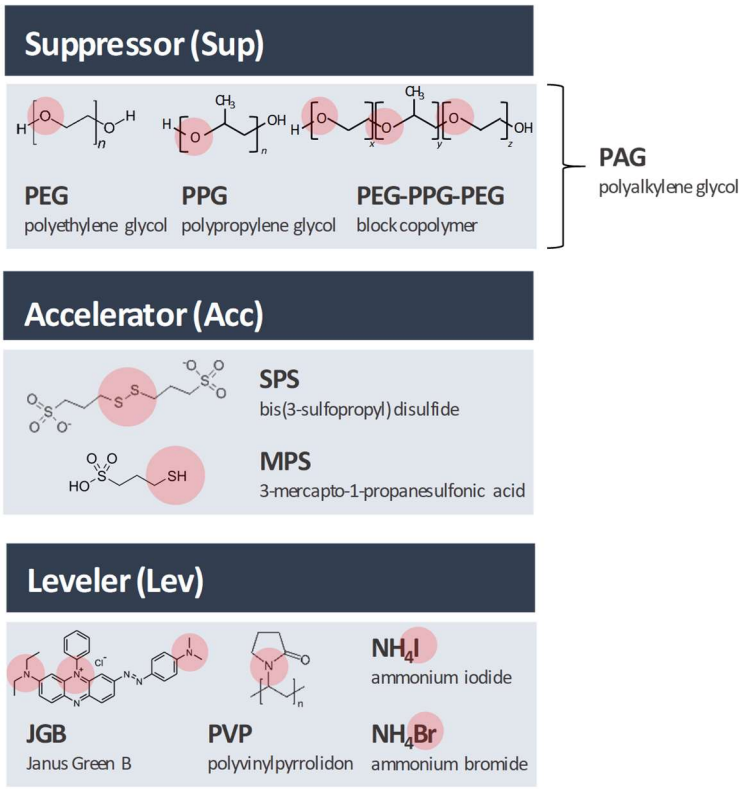

Figure 1.4. Structures and effective functional groups of various suppressors, accelerators, and levelers.

1.3. Degradation of Cu electrodeposition process

1.3.1. Degradation of accelerator and its effect on Cu electrodeposition

Cu electrodeposition process contains numerous chemical species, and undesirable chemical/electrochemical reactions with physical incorporation into the deposit could degrade the bath chemicals.[63, 64] SPS, the representative accelerator, is decomposed into MPS and 1,3-propane disulfonic acid (PDS).[65]

$$SPS + 2H^+ + 2Cu^+ \rightleftharpoons 2MPS + 2Cu^{2+} \quad \text{(Eq. 1)}$$

$$SPS + O_2 + H_2O \rightarrow PDS + MPS + H^+ \quad \text{(Eq. 2)}$$

The first reaction (Eq. 1) occurs reversibly through the dissociation of the disulfide group in SPS, but the second reaction (Eq. 2) occurs through various irreversible oxidation reactions. MPS forms a thiolate complex with Cu^+ during Cu electrodeposition process, and can be recombined into SPS through a reaction with Cu^{2+}, whereas PDS is irreversibly produced, causing accumulation in the electroplating solution, as described in Figure 1.5. PDS itself has no effect on the electrochemical reduction rate of Cu^{2+}, but as SPS is consumed to PDS, the concentration of the accelerator in the electrolyte decreases, and thus the filling performance and physical properties of the deposit could

be impaired.

The decomposition behavior of SPS changes under various conditions.[66] When the cathode is Cu, SPS reacts with Cu^{+} formed through the reaction between Cu of the electrode and Cu^{2+} (comproportionation reaction, $Cu + Cu^{2+} \rightleftharpoons 2Cu^{+}$) in the electrolyte in open circuit conditions to form $Cu(I)MPS^{-}$ complex, and is further converted into PDS through oxidation. At this condition, no chemical reaction is expected at the iridium oxide (IrO_2) anode, so the SPS is not decomposed. When the circuit is closed in an electrolytic system composed of Cu cathode and the insoluble anode, it is possible to observe SPS decomposition with the same rate at the cathode and the anode. This is because SPS is decomposed at the anode due to Cu^{+}, which is produced by reducing Cu^{2+} in the electrolyte to Cu^{+} at the electrode where the electron source comes from the cathode due to the spontaneous oxidation of Cu to Cu^{2+} or Cu^{+} at the electrode. In the electrolytic situation, a constant rate of SPS decomposition is observed at the cathode regardless of the intensity of the applied current density, which means the decomposition behavior of SPS is mainly dependent on the chemical pathway rather than the electrochemical pathway. In the anode, because SPS directly participates into the oxidation reaction (Eq. 3), rapid consumption of the accelerator occurs.

$$SPS^{2-} + 6H_2O \rightarrow PDS^{2-} + 10e + 12H^{+} \quad \text{(Eq. 3)}$$

The overall degradation of SPS in various electrochemical conditions is summarized in Figure 1.6.

1.3.2. Degradation of suppressor and its effect on Cu electrodeposition

PEG is not decomposed even under harsh solution conditions below pH 1. However, it was observed that PEG is degraded during the Cu electrodeposition process through which electric current flows, and is cleaved into PEG with a smaller molecular weight (MW) during this process. In general, the smaller the MW, the weaker the inhibition strength in Cu electrodeposition even at a mass concentration containing same amount of monomer units, and this cannot guarantee the quality of deposits formed after the deterioration. Previous research has shown that hypochlorite ion (OCl^-) could be electrochemically formed at the anode during Cu electrodeposition, and the ion contributes to the formation of hydroxyl radicals (·OH). PEG internal radicals are generated due to hydrogen abstraction in PEG by the hydroxyl radicals, followed by scission and complex radical decomposition of C – O bonds, as in Figure 1.7.[67] The PEG-PPG-PEG (EPE) copolymer (MW: 1,100 g/mol) also exhibits similar behavior. As Cu electrodeposition proceeds, it is fragmented into EPE with a smaller MW, and the

terminal group is converted into aldehyde, formic ester, and ketone as reported in previous studies that.[68]

Like SPS, PEG exhibits different decomposition behavior observed at the Cu cathode and IrO_2 anode under open circuit, closed circuit, and electrolytic conditions.[69] In open circuit conditions, PEG is decomposed only at the cathode, which is explained by the hydroxyl radical formed by Cu^+, while no degradation of PEG was observed in the insoluble anode. In the closed circuit situation, the decomposition behavior of PEG occurs at a similar rate for both the cathode and anode, and as in the case of SPS, electrons generated by the oxidation reaction of the cathode move to the anode and reduce Cu^{2+} to Cu^+, thereby forming hydroxyl radicals, which cause the decomposition of PEG at the anode. In the electrolysis process, the rate of PEG decomposition at the cathode and the anode is different, which is described by the fact that PEG is degraded at the cathode due to Cu^+ and the decomposition of hydroxyl radicals at the anode due to water splitting. The overall degradation of PEG in various electrochemical conditions is summarized in Figure 1.8.

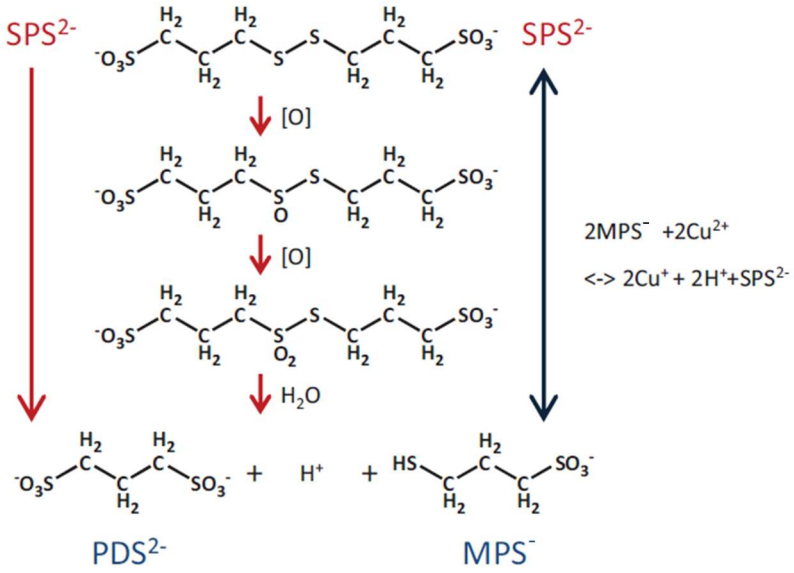

Figure 1.5. Decomposition pathway of SPS. (ref. 65)

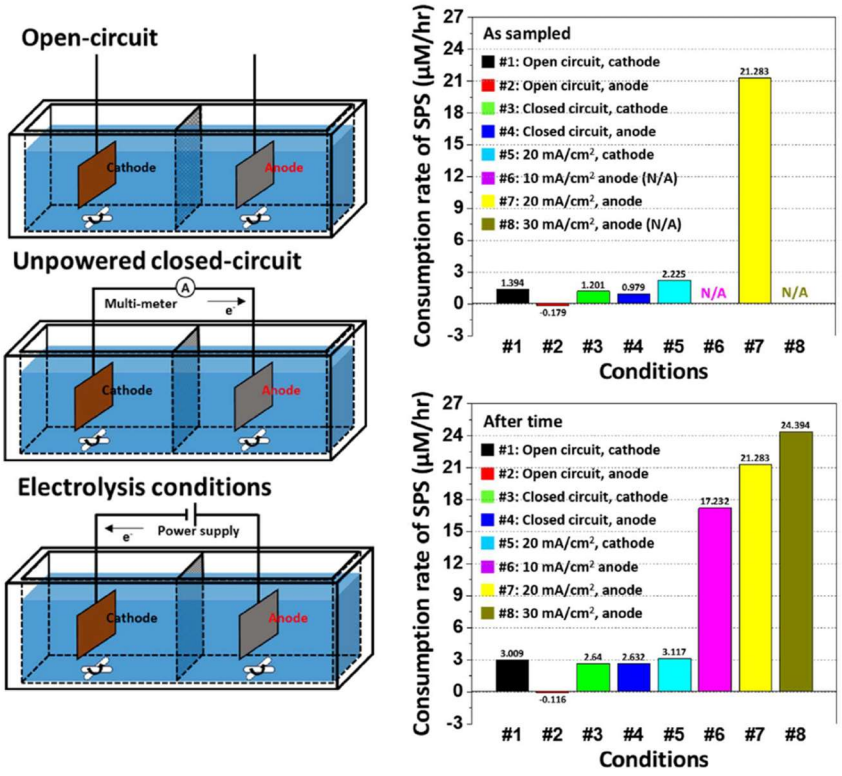

Figure 1.6. Decomposition rate of SPS at various electrochemical conditions. (ref. 66)

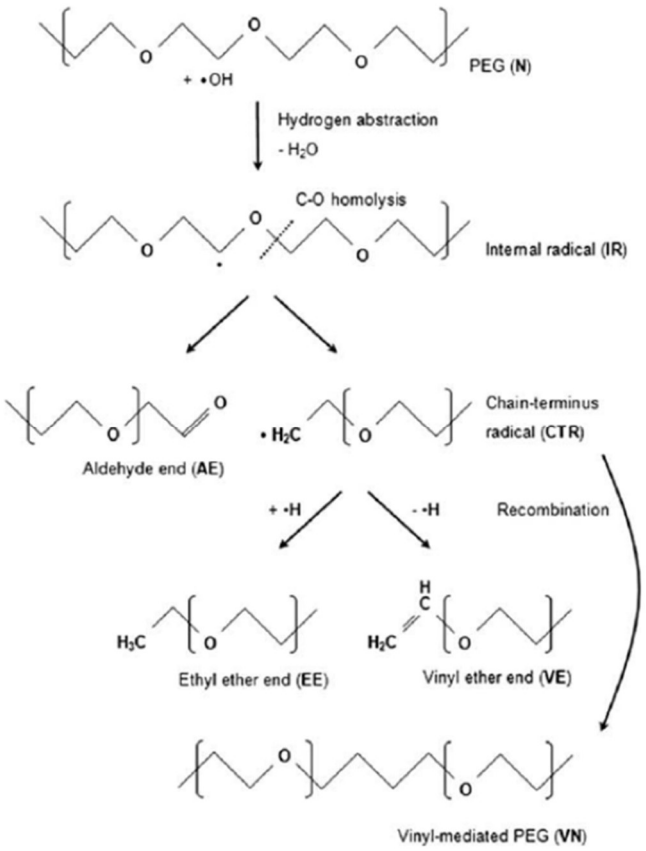

Figure 1.7. Decomposition pathway of PEG due to the hydroxyl radical. (ref. 67)

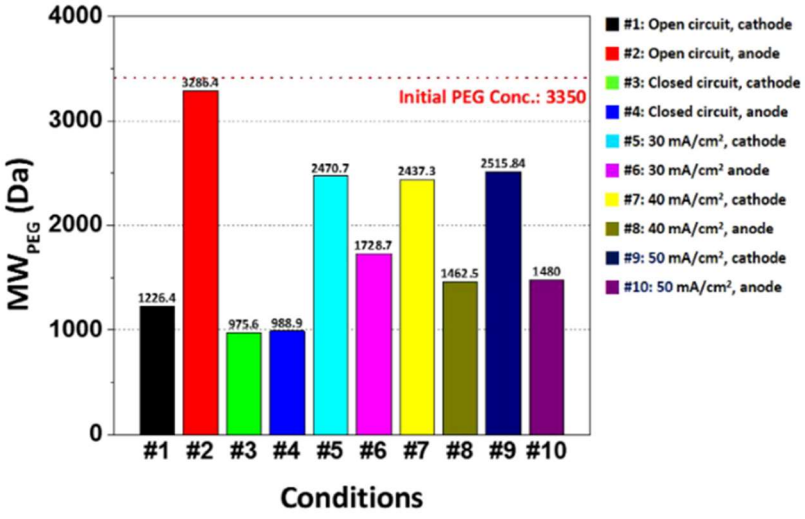

Figure 1.8. Decomposition rate of PEG at various electrochemical conditions. (ref. 68)

1.4. Electrochemical monitoring: Cyclic voltammetry stripping

The degradation causes the decrease in additives' concentrations, and the byproducts are formed in Cu electroplating bath. The concentration of the additives critically decides the electrochemical behavior of Cu deposition and the deposit property, and therefore in the electroplating industry, it is tightly monitored and controlled on a daily basis. Therefore, accurate monitoring of additives followed by precise feedback ensures the solution reliability during the long-term plating operation. Voltammetry or stripping voltammetry method has been widely researched as a monitoring tool for the concentrations of metal ion or organic chemical species. Cyclic voltammetry stripping (CVS) adopts similar voltammetric approaches in monitoring metal plating baths, but concentrates on the stripping charge in the cyclic voltammogram. Additives change the rate of Cu electroplating, and by this means, the type and concentration of the additives affect the stripping charge, which represents the electroplating rate. In previous research, various quantitative methods for determining the concentration of SPS/MPS couple,[70] thiourea,[71] and the average molecular weight of PEG using CVS have been proposed.[72]

1.4.1. Conventional CVS analysis

Conventional electrochemical stripping analysis is one of methodologies in an analytical chemistry based on voltammetry and potentiometry which is used to quantitatively measure the concentration of metal ions in a solution. When a potential ramp is applied to a positive potential after the electroplating at a negative potential, a stripping current peak is observed at the electrochemical oxidation potential of each metal. Since the standard electrode potential is different for each metal, peak separation occurs in the stripping process even if various metal ions exist in the solution, and through this, the type and amount of metal present in the solution can be specified. Stripping voltammetry is limited to metal ions which directly participate into the electrochemical reactions, and has a limitation in specifying its type and quantity. Unlike stripping voltammetry, CVS uses CV analysis integrating the electrodeposition and stripping step. In potential cycle, when the potential reaches the onset potential of metal deposition, electrodeposition starts, and in the return sweep, stripping takes place past the onset potential. The CVS method is more suitable for monitoring the concentrations of additives in Cu electrodeposition system which control the reduction rate of metal ions by adsorbing on the electrode surface, rather than metal ions directly participating into the electrochemical reduction reaction. The stripping charge observed in the controlled potential range means the rate of electrodeposition at the composition of the

plating solution (Figure 1.9), and the stripping charge changes according to the type and amount of additives. Therefore, from the change in stripping charge against the concentration of the additive as a calibration curve, which is obtained by using the standard additive, the concentration of an additive could be determined.

1.4.2. CVS analysis for accelerator

When the target solution is mixed (addition volume: V_T) with the base solution (volume: V_b) after measuring the stripping charge for the base solution (Q_b), the larger stripping charge (Q) would be detected by the effect of SPS in the target solution, and thus, $Q - Q_b$ is calculated. As the standard solution with known concentration of SPS (C_A) is added, the determined Q increases and exhibits linearity under certain conditions. At this point, the addition volume of the standard solution satisfying $Q - Q_b = 0$ could be predicted by linear approximation. As in the Figure 1.10, the volume V_i means the imaginary negative addition volume of the SPS standard solution when the stripping charge is same as the stripping charge of the base solution where no SPS is contained. From this value, the concentration of SPS could be determined in the target solution (C_T) with the equation in the Figure 1.10. The equation implies that the amount of SPS in V_T

of the target solution is same as the amount of SPS in V_i of the SPS standard solution.

1.4.3. CVS analysis for suppressor

Figure 1.11 shows the conventional dilution titration (DT)-CVS process to determine the concentration of EPE. (1) A base solution (volume: V_b) is dosed into the CVS bath, before the analysis is started. CV analysis is conducted, and the stripping charge of the base solution (Q_0) is evaluated. (2) Standard solution, which contains a known amount of a suppressor (concentration: C_S), is dosed into the base solution. (3) The CV analysis is carried out again. The stripping charge of the base solution with the added standard solution (Q) is evaluated. The whole procedure in steps (2) and (3) is repeated several times until the Q/Q_0 value decreases significantly, due to the effect of the suppressor. After the same Q/Q_0 plot is obtained from the target solution, the evaluation value is interpolated to determine the addition volume of the standard solution (V_S) and target solution (V_T). The equation implies that at the same evaluation value, concentration of EPE in the standard solution at the addition volume of V_T mixed with the base solution is same as the concentration of EPE in the target solution (C_T) at the addition volume of V_T mixed with the base solution. Utilizing the volume values and the equation, the

concentration of the suppressor in the target solution could be predicted.

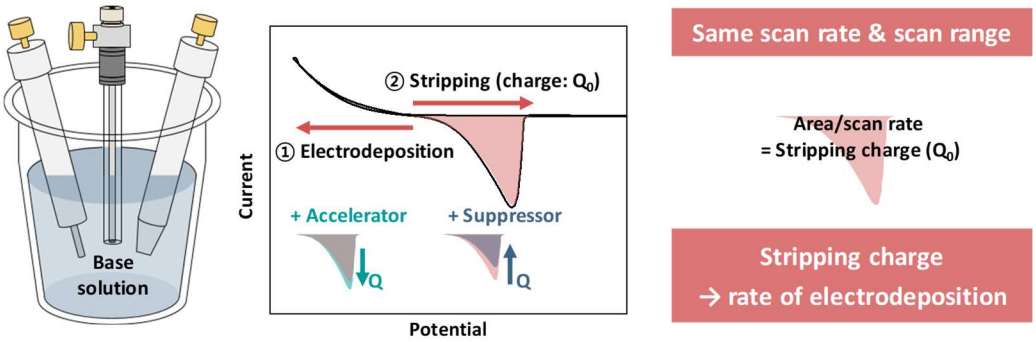

Figure 1.9. Scheme of conventional CVS analysis for determining additive concentration.

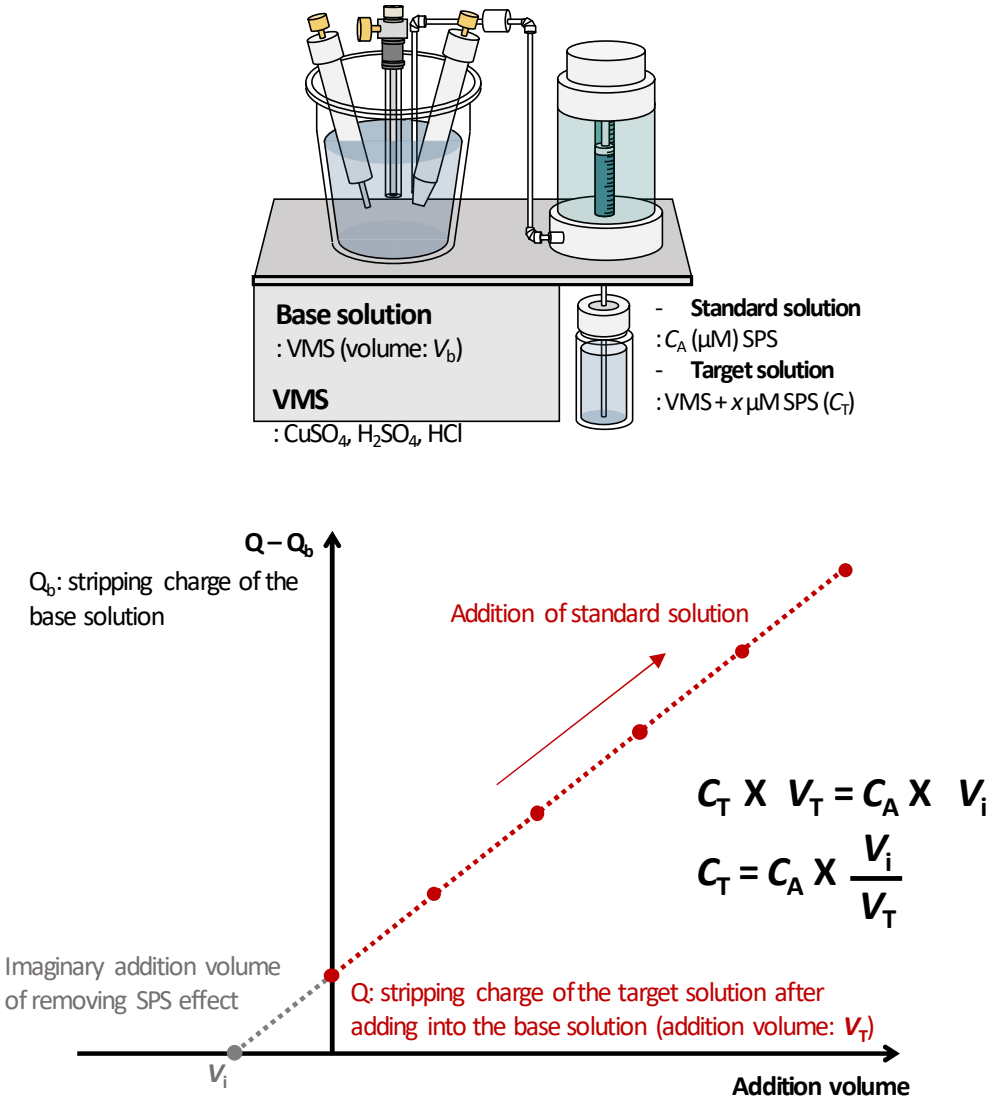

Figure 1.10. Scheme of determining SPS concentration using CVS analysis.

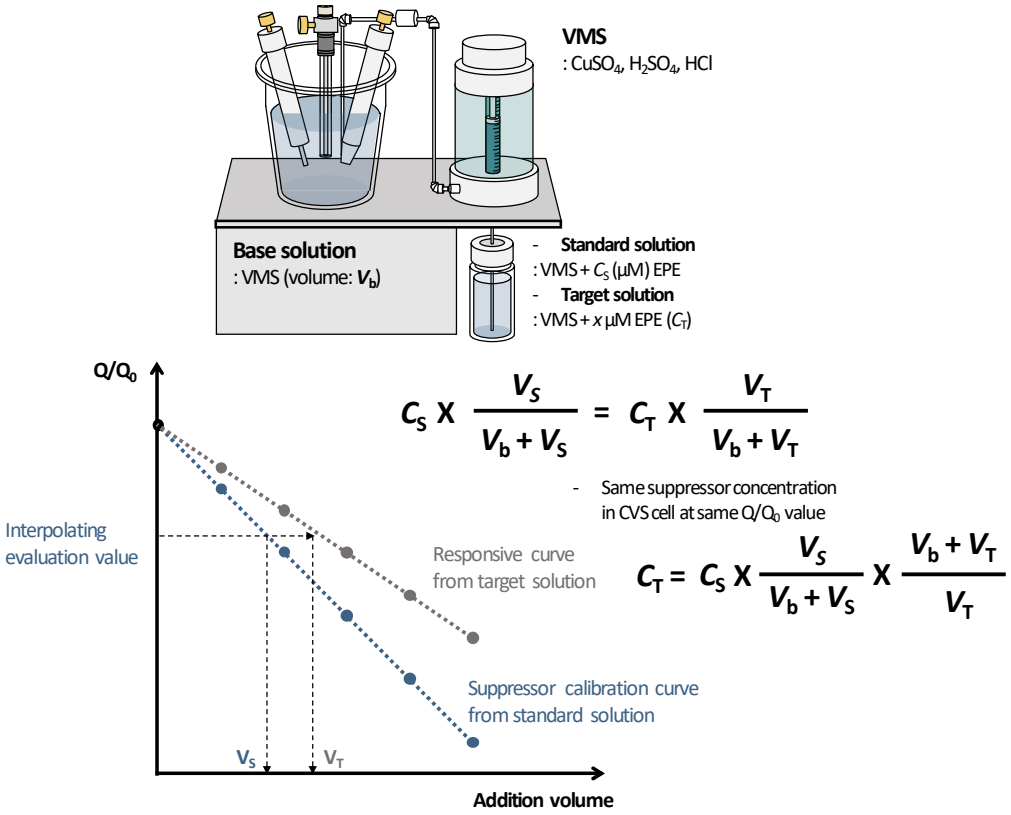

Figure 1.11. Scheme of determining EPE concentration using CVS analysis.

1.5. Machine learning for chemical system

Machine learning is a technology that allows a computer to learn knowledge from data by itself. It enables a system to respond from an input based on optimization of a statistical model through a large amount of data and computing power, and has attracted attention again as the recent rapid advance in hardware performance and the usability improvement in big data.[73-77] The superiority of machine learning over other problem-solving techniques comes from building a model based on data created from the system, not completely understanding how it works, and facilitating the solution itself to adapt to a change raised in the system by learning the data. For instance, machine learning could deeply affect the progress in speech recognition and computer vision by its data-driven approach, rather than understanding the cognitive system itself, because of too complex operating mechanism of human auditory and visual recognition, thereby increasing practical application such as natural language processing and image processing. In chemistry field, machine learning has been used in molecular and material science to guide chemical synthesis, assist multi-dimensional characterization, and enhance theoretical chemistry.[78] In addition, the chemical system itself could be disclosed by analyzing the optimized model learned from numerous data, providing the

unexpected insight to a chemist.

1.5.1. Property of electrochemical analysis

Monitoring of additives is performed by electrochemical analysis, which provides mass information from the system at once. LSV, CV, and chronoamperometry applies electrical potential perturbation to the system and extracts knowledge from the current signal measured in the system, while chronopotentiometry obtains information by applying a current perturbation to the system. In the case of analyte accompanying electron transfer, the generated signal is related to the quantitative information of the analyte, thereby enabling the estimation of the concentration of the analyte through the intensity of the signal. However, in the case of chemical species which do not directly participate in the faradaic process of the electrochemical reaction, such as additives in the Cu electrochemical deposition system, it is difficult to obtain quantitative information precisely from the signal, because the intensity of the signal generated during the electrochemical analysis is consistent when the concentration of Cu^{2+} in the standard analytic solution is constant. Instead, the quantitative information, such as concentration, of an additive could be determined through the change of the rate of

electrochemical reaction involving the analyte. As mentioned above, additives are involved in the Cu^{2+} reduction by adsorbing on the substrate and complexing with Cu^{2+}/Cu^{+}, resulting in the change of the rate of electrochemical Cu^{2+} reduction. Therefore, when the same perturbation is induced, the intensity of the electrochemical signal generated in the system depends on the concentration of the additive, even if the concentration of Cu^{2+} is constant. Accordingly, by using a standard additive solution with known concentration, a calibration curve of the signal change as a function of the concentration of the additive could be obtained, and through this, various methods of estimating the concentration of the additive in Cu electrochemical deposition system have been attempted.

1.5.2. Application of machine learning to electrochemical analysis

This approach exhibits the feasibility that quantitative information could be determined even for chemical species which do not directly participate in the electrochemical reaction, but when the Cu electrochemical deposition system contains various types of additives, it becomes difficult to estimate which additive affects the electrochemical signal generated in the analysis since each additive has a complex effect

on the rate of Cu^{2+} reduction. In other words, in a complex electrochemical system, the signal-to-noise ratio (SNR) for a particular additive decreases, making it impossible to selectively determine the concentration of the additive. In addition, in order to select an appropriate electrochemical method and conditions for the analysis, it is necessary to completely understand the Cu electrochemical deposition system, because the degree to which each additive affects the rate of Cu deposition depends on the chemical/electrochemical conditions, and it becomes difficult to extract meaningful information from the analysis conducted without understanding the mechanism of the system. As a result, this problem arises because the system is entangled with a complex operating mechanism and it is impossible to fully understand how the response to a potential or current perturbation occurs. Machine learning is an applicable approach as a solution to the problems caused by the complexity of these systems. When combining the superiority of electrochemical analysis with machine learning, it is possible to build a model which could extract quantitative information by learning numerous electrochemical data on system variables, and it is expected that the understanding of the operating mechanism of the electrochemical system could be improved through analyzing the optimized model.

1.5.3. Various machine learning algorithms for electrochemical analysis

k-nearest neighbors (k-NN) is the simplest machine learning algorithm. Learning in k-NN algorithm means just storing the training dataset, and the prediction for a new data points is conducted by finding the closest data point in the training dataset. In other words, finding the 'closest neighbor' is how the model predicts. The way k-NN algorithm works is to determine the training data point closest to a test data point by measuring, in general, Euclidean distances between the data points, and the result, the prediction of the test data point, is the same as the target of the nearest training data point. The representative parameter, *n_neighbors*, refers to the number of neighbors referenced in comparing the distances, and if it is greater than 1, the predicted value is returned as the average of the output values of the nearest *n_neighbors* neighbors. k-NN algorithm has easy working process and fast building, and shows reasonable performance without any adjustment. k-NN algorithm is a basic algorithm which is worth using before applying more complex machine learning techniques. The downside of the algorithm is the slow prediction when the large number of features or data points are used.

Linear model has been widely used in machine learning-based problem solving. It yields a prediction using a linear function optimized through the input features of training dataset. The general prediction equation for a linear model is

$$\hat{y} = w_0 \cdot x_0 + w_1 \cdot x_1 + \cdots w_\mathrm{p} \cdot x_\mathrm{p} + b \quad (\mathrm{Eq.}\, 4)$$

x_0 to x_p indicate the value for each feature of a data point, so the number of features in Eq. 4 is (p + 1). w_0 to w_p and b are the parameters of the model determined through training, implying the weight of the features on the predicted value, and $\hat{y}$ is the prediction output made through the model. There are several linear models for solving linear regression problems. These depend on how the model's parameters, w and b, are determined from the training dataset and how the model complexity is adjusted. Linear regression, or ordinary least square (OLS) estimation, is the simplest yet classic algorithm for regression problems. Linear regression selects w and b so that the mean squared error between the predicted and actual values obtained from the training data is minimal. The linear model works well when the number of features is large compared to the number of samples. For this reason, it is often used on very large feature dataset, but for lower dimensional dataset, other models show better generalization performance.

Decision tree is also widely used for classification and regression. It learns the hierarchical structure of if/else control statements which lead to a certain decision. Learning in decision tree involves a series of if/else questions which reach the correct answer most quickly, and in machine learning, these questions are called tests. Test is made in the same way as “Is the feature value *i* greater than the value *a*?” Observing the whole tree after learning is also helpful, but there are some useful features which can help you summarize the behavior of the tree simply. The most commonly used summary method is feature importance. Feature importance ranks how important each feature is in building a decision tree. Each feature has a value between 0 and 1, where 0 is the feature that was never used to build the tree, and 1 is the feature that perfectly predicts the target. Decision tree has two advantages over other algorithms. First, the resulting model is easy to visualize and can be understood by non-experts. Second, it is not affected by data scaling. That is, no normalization or standardization is required. Decision tree, in particular, works well with data with features that have completely different scales, or with both binary and continuous features. The disadvantage of decision tree is that even with pre-pruning, it tends to do overfitting and shows poor generalization performance.

Artificial neural network (ANN) is a statistical learning algorithm inspired by biological neural networks which has recently attracted attention again with the revival of deep learning. ANN basically approaches the prediction similar to linear model, but is composed of a number of perceptrons in hidden layers between the input and the output layers. A perceptron is calculated by multiplying perceptrons (or input) of the previous layer by weight respectively and then adding the results. Then the result is substituted into an activation function, which distinguishes whether the signal from the previous perceptrons has a magnitude greater than a certain value like a neuron. The multilayer perceptron (MLP) is composed of various layers between the input and output, which are composed of a number of perceptrons respectively. ANN optimizes the weights between the perceptron layers using training dataset through backpropagation. ANN has the disadvantage of taking a long time to train, but the time it takes to predict after the training is very short, supported by its many applications in real-time prediction. ANN also could capture information contained in a large amount of data and is superior to other machine learning algorithms.

1.6. Purpose of this study

The determination of I^- has been widely researched in many fields. Using potentiometric method with iodide-selective electrodes or a direct stripping voltammetric method could be a good option for monitoring I^- in Cu plating bath. Those methods show short and direct determination of I^- in various aqueous samples. However, those methods are appropriate for a relatively mild chemistry (pH > 2) without severe ionic strength in contrast to high acidic solutions with high Cu source concentration used in Cu electrodeposition. Also, Cu plating procedure accompanies fluctuation of pH of the solution, which could lead to the error. Therefore, the research on the degradation of I^- and its monitoring in the conventional acidic Cu plating baths by using CVS is necessary and further study is being required to use I^- as a future leveler. The chemical/electrochemical reactions relevant to I^- consumption during the Cu electrodeposition and the influences of its by-products from those reactions are investigated. An electrochemical method to detect the precise concentration of I^- (C_I) in a Cu plating bath based on the responsive curve (RC)-CVS technique is also suggested.

The limitation of CVS analysis originates in the presence of complex additives: the other co-added additives can interfere with the pure action of the target additive, and in

turn, become a noise source during analysis, resulting in a possible risk when analyzing baths for damascene or TSV filling process, where the suppressor contents are typically under 100 μM. However, from the understanding of the chemical and electrochemical behavior of additives, selective and quantitative determination of additive concentration is available. In this part, a novel method is suggested that enables high-accuracy analysis of suppressor concentrations at very low concentration range (~50 μM), free from noise by accelerator. This method is based on the suppressor-Cu^{+}-I^{-} complex that is strongly adsorbed on the electrode surface with less displacement by SPS in wide ranges of potential. The optimal voltammetry conditions for minimizing the disruption by SPS are also discussed.

In the third part, the concentrations of PEG and Cl^{-}, essential additives generally used in a Cu electrochemical deposition system, are predicted through an ANN, one of the methodologies of machine learning, optimized by CV data on the additive concentrations. Cl^{-} first adsorb to the substrate during the Cu electrochemical deposition and act as a traction to induce strong adsorption of PEG, inhibiting the physical access of Cu^{2+} to the substrate. This PEG-Cl^{-} inhibition layer increases the energy required for Cu^{2+} reduction and slows down the rate of Cu electrochemical deposition, and it is very challenging to determine each concentration selectively due to the complementary effects of the two

additives. In addition, as the electrochemical deposition process is repeatedly performed, PEG is decomposed into smaller PEG fragments. Polymers such as PEG have a physicochemical parameter such as MW in addition to concentration, which complicates the system. PEGs with different MWs exhibit different electrochemical behavior even at the same mass concentration (the same number of ethylene glycol units) in Cu electrochemical deposition. Particularly, PEG having a small MW (i.e., MW = 200 g/mol) has little effect on Cu^{2+} reduction even if a sufficient amount of Cl^- is present, so it is impossible to determine the concentration through an electrochemical analysis. By shifting the vertex potential in CV and introducing iodide ion (I^-) as a secondary halide ion, the SNR of each PEG and Cl^- enhances and the performance of ANN model for predicting each additive concentration improves.

CHAPTER II

Experimental

2.1. Aging experiment and effect of degradation on TSV filling

In Chapter 3.1.1, the degradation of I^- during Cu electrodeposition was performed in order to specify the byproduct of I^- and confirm its consumption. The degradation test proceeded with 2 L of a Cu acidic plating solution which contained 400 μM of NH_4I as an additive in the Cu electroplating solution consisting of 1.0 M $CuSO_4$, 0.5 M H_2SO_4, and 1.4 mM HCl (virgin makeup solution, VMS in the chapter). The Cu plate (cathode) and IrO_2/Ti (anode) with the same dimension of 62.5 mm×80 mm×1 mm (length × width × thickness in both sides, geometric area: 100 cm^2) were immersed into the electrolyte in the electrochemical cell (length × width × height: 120 mm×120 mm×150 mm). The distance between the electrodes was 60 mm and no electrodes were isolated (Figure 2.1(a)). The cathode was pretreated by dipping in 0.02 M citric acid and 0.03 M KOH solution for 2 minutes and the anode was rinsed with deionized (DI) water before the experiment, in order to remove native oxide. The current (1 mA/cm^2, same as TSV filling condition) was applied for 4,400 s using a direct current (DC) power supply (XG 33-25, Sorensen). After the degradation test, the insoluble white particles formed on the cathode.

The electrode was rinsed with DI water and the particles were collected from the DI water by using a pipette. The particles were dispersed on a Ti wafer (370 nm Ti/Si) and dried before the analysis. The particles on the wafer were further confirmed with field-emission scanning electron microscopy (FE-SEM) as well as energy-dispersive spectroscopy (EDS) analysis (MERLIN Compact, ZEISS).

The effect of the degradation of I^- on the TSV filling performance was certified by TSV filling. The TSV wafer included a micro-scale via with a depth of 60 μm and a 5 μm diameter (aspect ratio: 12), where the Cu (600 nm)/Ta (200 nm) seed was deposited. The TSV wafer was loaded in a home-made holder which exposed active area of 1.0 cm^2 and was physically connected to the rotator, as in Figure 2.1(b). The working electrode was rotated with 1,000 rpm using rotator (Model 616A, Princeton Applied Research) during the filling process. VMS with 10 μM SPS, 50 μM EPE (MW: 1,100 g/mol in the chapter), and x μM NH_4I (x = 100, 200, 300, and 400) were used to test the effects of the concentration of I^- (C_I) and VMS with 10 μM SPS, 50 μM EPE, and 400 μM NH_4I; excess I_2 (C_{I_2} = 800 μM) or CuI (C_{CuI} = 800 μM) confirmed the effect of I_2 and CuI each, as a by-product. The electrochemical system for the TSV filling consisted of the working electrode (the TSV wafer, active area: 1 cm^2), the counter electrode (Cu wire, diameter: 2 mm, length: 30 mm), and the reference electrode (Ag/AgCl/KCl (sat'd)). The reference

electrode was located beside 20 mm from the working electrode and the counter electrode was located below 10 mm from the working electrode. A current density of 1 mA/cm^2 was applied for 2,200 s during the TSV filling.

2.2. Electrochemical analysis

In Chapter 3.1.2, the electrochemical analysis was conducted for the confirmation of the effect of additives and chemical/electrochemical optimization for CVS analysis. For the determination of I^- concentration in Cu electrodeposition system, commercial CVS equipment (797 VA Computrace, Metrohm), consisting of a three-electrode electrochemical cell (working: Pt disk (active area: 3.14 mm2), counter: Pt rod (diameter: 2 mm, length: 14 mm) and reference: Ag/AgCl [3 M KCl]) and an automatic dosing system (MVA12, Metrohm), was used. The distance between working and counter electrode and that between working and reference electrode were fixed at 10 mm. Before analysis, the working electrode was cleaned by applying 1.575 V for 10 s. A base solution, comprising VMS, 2.88 mM PEG (MW: 3,350 g/mol) and 19.2 mM SPS, was utilized throughout the experiment. To confirm the effect of the RDE rotating speed and the vertex potential, each parameter was varied between 0 rpm to 2,000 rpm and –0.1 V to –0.4 V. The Q/Q_0 change (Q_0: the stripping charge of the base solution, Q: the subsequent stripping charge after addition of a dosing solution) with the addition of the standard solution (VMS with 10 μM SPS, 50 μM EPE, and 400 μM NH_4I) was recorded

as a function of the C_I. The effective coverage ($\theta_{eff,I}$) was estimated with various conditions. $\theta_{eff,I}$ was defined as

$$\theta_{eff,I} = 1 - \frac{i_{I^-}}{i_{sat}} \quad (Eq. 5)$$

where i_{sat} was the current measured at a given potential range only when the base solution existed in the CVS bath, and i_{I^-} was the current at same range after adding the standard solution to the base solution. C_I was controlled from 7.55 μM to 53.3 μM by the dosing system. The effects of scan rates (100, 75, 50 mV/s) and rotating speeds of the electrode (400-2,000 rpm) were tested by varying them.

In Chapter 3.2, for the optimization for selective determination of suppressor concentration, various electrochemical variables were tested in the CVS system, using CV and LSV. The selected suppressor concentration (C_S) in CVS bath to be used in the electrochemical analyses was 2 μM, based on the situation where the 50 μM EPE (MW : 1,100 g/mol in the chapter) was diluted into 1.0 M $CuSO_4$, 0.5 M H_2SO_4, and 1.4 mM HCl (VMS in the chapter). The selected accelerator concentration (C_A) was 10 μM, considering the dilution of target solution containing up to 250 μM of SPS, which could exert strong interference by SPS. NH_4I was used as I^- source, considering negligible effect of the cation, NH_4^+, on the CVS analysis, and its concentration was 400 μM (C_I =

400 μM). The combination of additives in Cu electroplating solution was chosen as EPE/EPE-SPS and EPE-I^-/EPE-SPS-I^- with the change in vertex potential of –0.3 to –0.35 V and scan rate of 10 to 100 mV/s. The effect of scan rate on the ratio of the formation of Cu/CuI was further proved quantitatively by simulating the CVS analysis in an electroplating system. Au wafer, composed of Au (130 nm)/TaN (200 nm)/Ta (50 nm) on Si wafer was fixed on teflon rod by chemical-protective waterproof tape and the electric contact was made using Al foil. The active area of 0.25 cm^2 was exposed to the Cu plating solution compoased of VMS with C_A = 10 μM, C_S = 2 μM, and C_I = 400 μM. This holder was chosen as a working electrode, and rotated during the electroplating at 2,000 rpm, using a rotator (Model 616A, Princeton Applied Research). The electroplating was performed with CV method, sweeping from 0.05 to –0.35 V, and back to 0.05 V, selecting a scan rate from 10 to 100 mV/s, as conducted in the previous experimental section. The characterization step to confirm the morphology and atomic composition of the deposits was conducted using FE-SEM and EDS analysis (MERLIN Compact, ZEISS). The additional surface characterization was performed to confirm the effect of I^- on Cu deposit under analytic environment using X-ray diffractometer (XRD, D8-Advance, BRUDER MILLER Co.) and X-ray photoelectron spectroscopy (XPS, SIGMA PROBE, ThermoFischer). The reference (without I^-) sample was prepared by

using same method except adopting VMS as a plating solution. In the LSV analyses, combinations of EPE, SPS, and I^- were used to verify the effect of I^- on the CVS analysis in the optimized electrochemical condition. Furthermore, the effect of higher C_S should be confirmed to guarantee a wide determination range of C_S because the displacement of the EPE by SPS can also be affected by the amount of suppressor. The C_S in CVS bath was controlled from 2 to 10 μM, and cyclic voltammograms with and without I^- were compared to confirm how the higher C_S could affect the SPS-inhibiting power of I^-.

In Chapter 3.3, in order to investigate the reason for the improvement of the signal responsibility of low MW PEG due to the addition of I^- in PEGs & Cl^- one pot monitoring using deep learning, the effect of I^- on the Cu CVS analysis was studied through electrochemical analysis. Same CVS system, consisting of a three-electrode electrochemical cell (working: Pt disk (active area: 3.14 mm2), counter: Pt rod (diameter: 2 mm, length: 14 mm) and reference: Ag/AgCl [3 M KCl]) and an automatic dosing system (MVA12, Metrohm) were used. At first stage, the effect of I^- on Cu electrodeposition and stripping was confirmed through CV analysis. The potential sweep range was set from 1.575 V to –0.2 V, and again to 1.575 V with scan rate of 0.1 V/s. The base electrolyte was composed of 1.0 M $CuSO_4$ and 0.5 M H_2SO_4 (VMS in the chapter) with the volume of 50 mL. NH_4I, the I^- source, was repeatedly dosed into the

base electrolyte by the dosing system and the concentration of I^- in the CVS cell was controlled from 0 to 500 μM. To the next, in the new base electrolyte where 500 μM I^- was added to the previous base analyte, the cyclic voltammogram was observed as each PEG and Cl^- was added. The MW of PEG used in this experiment is 200 g/mol and the concentration of the PEG was controlled from 0 to 335 ppm. The overall electrochemical analysis using CVS system is summarized in Figure 2.2.

2.3. CVS analysis

In Chapter 3.1.2, to determine C_I in the target plating bath, a RC-CVS analysis was performed as follows: (1) assessment of Q_0 from the CVS analysis of the base solution (volume: 52 mL), (2) measurement of Q after adding the standard solution to the base solution (addition volume: 1 mL), (3) consecutive repetition (seven times) of the procedure (2) to generate a response curve, (4) preparation of a new bath and the appraisal of Q_0 (5), evaluation of Q_t after adding the target solutions to the base solution (addition volume: 3 mL), (6) determination of C_I in the target solutions by interpolating the Q_t/Q_0 value to the response curve by using Eq. 6.

$$C_{\mathrm{I}} = C_{\mathrm{St}} \times \frac{x^*}{V_{\mathrm{T}}} \times \frac{V_{\mathrm{T}} + V_{\mathrm{V}}}{x^* + V_{\mathrm{V}}} \quad \text{(Eq. 6)}$$

where C_{St} was the known concentration of I^- in the standard solution (400 μM), V_T the addition volume of the target solution, x^* the addition volume value (3 mL) in the response curve at the same Q/Q_0 with Q_t/Q_0 obtained from the target solution, and V_V the pre-dosed volume of the base solution (52 mL). The reliability of this method was confirmed by testing the other target solutions comprising the VMS solution with x μM SPS, y μM EPE, and 250 μM NH_4I with the same CVS analysis. The method described above was applied to monitor C_I in a Cu plating bath for the TSV filling process. The

aged TSV filling solution was prepared by conducting the degradation test with a suppressor- and accelerator-free bath, as well as the subsequent addition of 10 μM SPS and 50 μM EPE to the solution. Applying the RC-CVS analysis at optimized conditions, the C_I in the aged Cu plating solution was determined and the consumed I^- added to the aged solution. The recovered performance of the solution was confirmed with the TSV filling.

In Chapter 3.2.2, the effect of SPS on the determination of the suppressor concentration (C_S) was simulated by using conventional diluting titration (DT)-CVS analysis. The block copolymer EPE was used as a target suppressor. In this experiment, 30 mL of VMS was used as the base solution. SPS concentrations in CVS bath were controlled from 0 to 1 μM to simulate the effect of the secondary additive. The standard solution consisting of the VMS and 50 μM EPE was successively added (0.5 mL) into the CVS cell containing VMS and SPS. The CV analysis was performed from +1.575 to –0.2 V, and again back to +1.575 V (vs. the reference electrode), with 100 mV/s scan rate, and 2,000 rpm rotation speed of the working electrode. The CVS bath temperature was controlled by thermostat at 30℃. The cyclic voltammograms was obtained from the CVS analysis explained above, and the charge consumed in the stripping region decreased as the C_S in the CVS bath increased. Using the optimized electrochemical

conditions, I^- was used as an inhibitor for SPS in modified CVS analysis to determine the suppressor concentration in two-additive copper plating solution. The determination was repeated with the change; instead of VMS, base solution containing VMS and 400 μM of I^- was used. Various Cu plating solutions, consisting of VMS, 50 μM EPE, and x μM SPS (x = 0, 10, and 100), were analyzed to confirm if a consistent response curve could be obtained, irrespective of C_A. Then, the target solutions consisting of the VMS and y μM EPE (y = 10 to 70), and 10 μM SPS were evaluated using the modified method.

In Chapter 3.3, in order to build a deep learning model for monitoring each concentration of PEG with respect to molecular weight and Cl^-, an aqueous base electrolyte containing 1.0 M $CuSO_4$, 0.5 M H_2SO_4 (VMS) was adopted for electrochemical analyses. PEG (MW: 200, 1,500, 3,350 g/mol), and HCl was used as an additive and their concentrations were controlled in a specific range: 0 to 335 ppm for PEGs (C_{PEG200}, $C_{PEG1500}$, and $C_{PEG3350}$: each concentration of PEG200, PEG1500, PEG3350) and 0 to 1 mM for Cl^- (C_{Cl}: concentration of Cl^-). CV analysis was performed by a CVS system (797VA Computrace, Metrohm) in a three-electrode configuration. A Pt rotating disk electrode (RDE) with a geometric area of 0.0314 cm^2 was used as a working electrode, and a Pt wire and Ag/AgCl [3 M KCl] as a counter electrode and reference electrode, respectively. Before starting analysis, the Pt electrode was

electrochemically pretreated between 0.5 V to 1.575 V (all the potential was applied with respect to the reference electrode) for 10 times with a scan rate of 1 V/s. Stabilization and equilibration was conducted by applying 1.575 V for 20 seconds to enhance the reproducibility. The rotating speed for the Pt RDE was controlled to 2000 rpm. CV was performed with sweeping the electrode potential from 1.575V to x V (x = –0.4 and –0.2) and then 1.575 V again with a scan rate of 0.1 V/s. In order to enhance the responsibility of low molecular weight PEG, 500 μM NH_4I is added in to the base electrolyte. All the additive concentrations were chosen randomly in order not to bias the learning model.

2.4. Machine learning

Figure 2.3 describes the overall machine learning process for predicting additive concentration from an electrochemical analysis. The data for machine learning consists of a vector containing the concentration of the additives to be used and a vector of the result of electrochemical analysis measured at the chemical composition. The purpose of machine leaning is to implement a model, which is able to output a concentration vector of the additives when inputting the electrochemical analysis result, and therefore, each result of electrochemical analysis in the dataset is labeled with the concentrations of additives. This type of machine learning is called supervised learning. As a method to collect data, CV in a three-electrode system was used, which applied the potential cycle between the working electrode and the reference electrode and observed the current measured between the working electrode and the counter electrode. In the standard analyte, the basis of the analysis, CV analysis in a controlled potential range is performed with random composition of the additives. PEG1500, PEG3350, and Cl^- is active, while the low MW PEG (PEG200) is relatively inactive in CV analysis. From the analysis, current-potential profile observed under the corresponding chemical composition represented by the concentration vector could be obtained. Potential is assigned as the

attribute of current, a feature value to be used for machine learning, and is not used for learning. Data preprocessing for machine learning was performed by standardizing the feature and target of the entire dataset sot that the mean is 0 and the standard deviation is 1, respectively. For example, if there are 3000 datasets for training, all 3000 current values at 1.575 V of CV is considered to be standardized. By standardization of values of each feature and target, the bias which the feature and target values themselves could give to learning was removed. The models used in the training were KNeighborsRegressor in neighbors module, LinearRegression in linear_model module, DecisionTreeRegressor in tree module, and MLPRegressor in the neural_network module of the scikit-learn package.[79] In the MLPReguressor, ReLU (rectified linear unit) function as the activation function, and the max iteration was 100,000, and the optimization process was performed according to the hidden layer size. The training was accomplished through cross validation, and the training dataset was divided into 5. 4 of the divided training dataset were used for training and the other was used for evaluation alternately to optimize the hyper parameter.

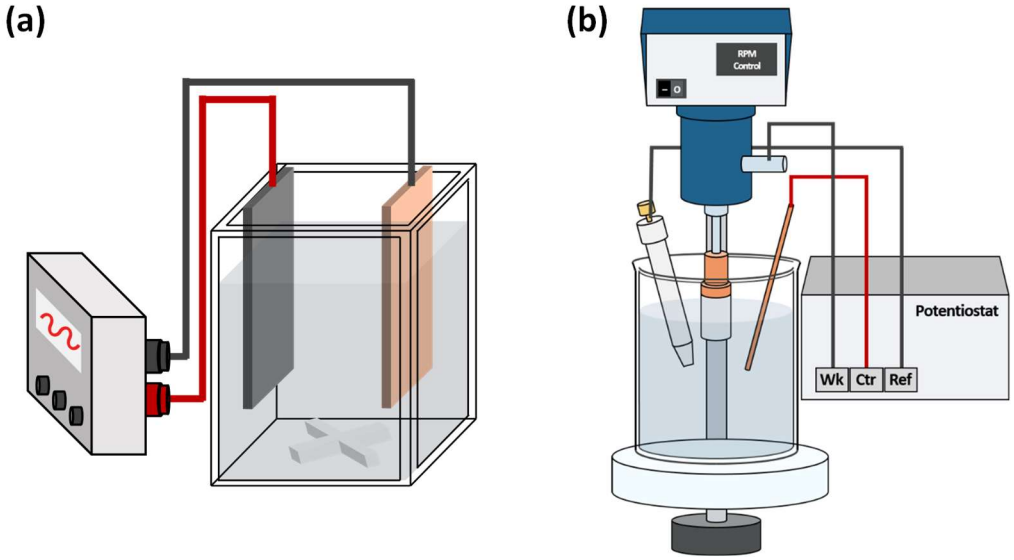

Figure 2.1. (a) Degradation system and (b) TSV filling system.

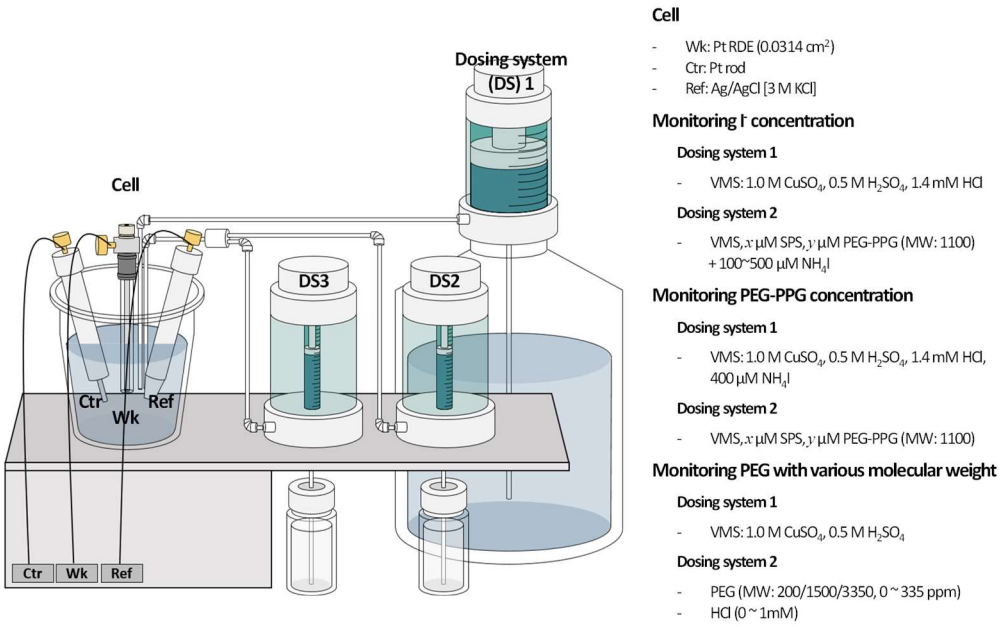

Figure 2.2. CVS system adopted for electrochemical analysis and additive monitoring.

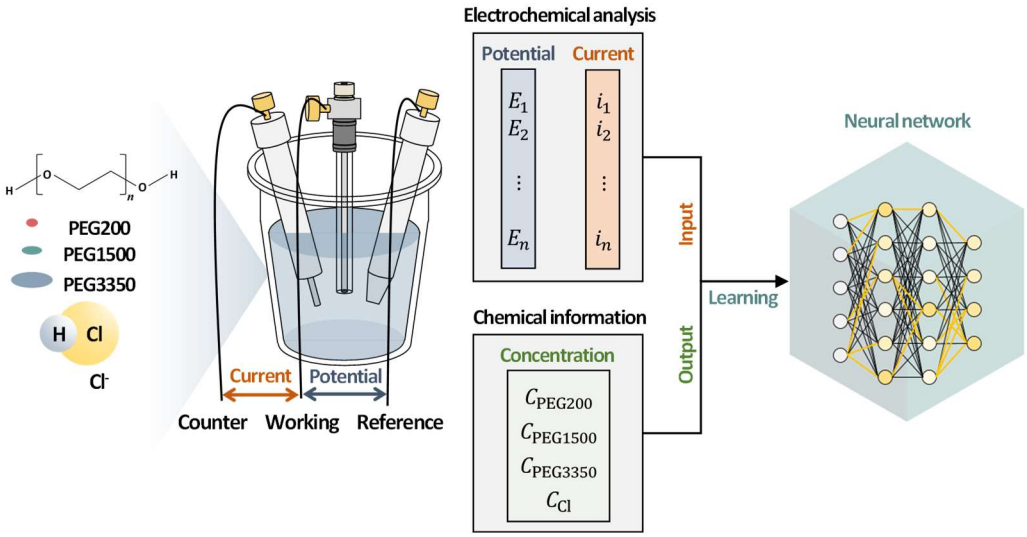

Figure 2.3. Scheme of machine learning process for electrochemical analysis of a Cu electrolyte containing PEG200, PEG1500, PEG3350, and Cl^-.

CHAPTER III

Results and Discussion

3.1 Effect of the degradation of I^- and its monitoring

3.1.1. The effect of the degradation of I^-

First, the by-products produced via I^--related side reactions were verified. After the degradation experiment at 1 mA/cm^2 for 4,400 s, the insoluble white particles, which were predicted as one of the by-products, were formed on the cathode surface. The FE-SEM image of the particles and corresponding EDS results are shown in Figure 3.1. The EDS analysis of the particles revealed that the particles contained the elements Cu and I with almost same atomic ratio (Cu: 28.6%, I: 30.3%), indicating the formation of CuI. CuI could be produced via the electro-reduction of Cu^{2+} to Cu^+, followed by the reaction between Cu^+ and I^-. Additionally, Cu^+ could be formed via the disproportionation of Cu^{2+} ($Cu^{2+} + Cu \rightleftharpoons 2Cu^+$) in an open-circuit condition when a copper plate was dipped into a Cu^{2+} electrolyte. In addition to CuI, I_2 could be theoretically produced as a by-product through the electrochemical oxidation reaction at the anode ($2I^- \rightleftharpoons I_2 + 2e$). In summary, as presented in Figure 3.2, I^- is thought to be consumed in three ways: the

chemical reaction with CuI at the cathode ($Cu^+ + I^- \rightarrow CuI$ (insoluble)), the electrochemical oxidation reaction at the anode ($2I^- \rightleftharpoons I_2 + 2e$), and the incorporation into growing Cu film at the cathode. Additionally, Palmer et al. reported that I_3^- could be formed via the chemical reaction between I_2 and I^-. Milenkovic and Stanisavljev also demonstrated that I^- reacted with H_2SO_4 and oxidized to I_2, even at an open-circuit condition, as in the following Eqs. 7 and 8.

$$I^- + H_2SO_4 \rightarrow HI + HSO_4^- \text{ (Eq. 7)}$$

$$2HI + H_2SO_4 \rightarrow I_2 + SO_2 + 2H_2O \text{ (Eq. 8)}$$

I^-, I_2, and I_3^- form equilibrium, and the theoretical equilibrium concentrations of I^-, I_2, and I_3^- at 25℃ are 360 μM, 14.5 μM and 3.65 μM, respectively, assuming the equilibrium constant of the reaction at 25℃ is 698[80] and the activity coefficient of each species is one. In summary, two major byproducts (CuI and I_2) and one minor byproduct (I_3^-) are expected to form during the operation of plating.

Changes in the filling performance from the conversion of I^- to CuI and I_2 were examined by controlling C_I, CuI, and I_2 (Figure 3.3). The filling features in Figure 3.3(a) to Figure 3.3(c) show that 400 μM of I^- led to void-free filled features whereas 300 μM

and 200 μM of I^- resulted in some voids at the bottom. When C_I = 100 μM, the void was propagated to the center as shown in Figure 3.3(d). Figure 3.3 (e), and Figure 3.3(f) display that CuI and I_2 rarely affected the filling capability, even at excess concentrations. It can be clearly inferred from these results that C_I was the critical factor for the filling capability, while CuI and I_2 in the Cu plating solution were less significant.

3.1.2. Electrochemical monitoring of I^- concentration using CVS analysis

Since C_I proved to be the only essential constituent, a further investigation to develop a way for monitoring it was carried out, based on the RC-CVS method. A base solution that exhibited a stable electrochemical response unaffected by any signal interference from the concentrations of co-added PEG and SPS was made. Because this solution contained excessive amounts of the suppressor (2.88 mM PEG (MW: 3,350 g/mol)) and the accelerator (19.2 mM SPS), its electrochemical response was insensitive to the concentrations of both the suppressor (C_S) and accelerator (C_A) species (Figure 3.4(a) and Figure 3.4(b)). During the plating operation, SPS was converted to MPS, while polyether suppressors fragmented to lower MW units. Therefore, the electrochemical

response of the base solution should be insensitive to MPS and to lower MW PEG as well as their parent additives. As shown in Figure 3.4(c) and Figure 3.4(d), all tested species (SPS, MPS, EPE, and PEG with various molecular weights) scarcely affected the Q/Q_0 values in the CVS analysis, which meant that the effects of those additives could be excluded in the CVS analysis for C_I.

Using the base solution and the standard solution, the electrochemical response of I^- was examined for various rotating speeds (Figure 3.5(a)) and vertex potentials (Figure 3.5(b)). Consistent with previous research, I^- showed a stronger inhibition effect on the Cu electrodeposition when the rotating speed increased (Figure 3.5(a)). Additionally, as shown in Figure 3.5(b), the Q/Q_0 drop's slope was high at –0.1 V (8.4/mM) and –0.2 V (7.8/mM) of the vertex potential but drastically reduced to 4.9/mM and 3.1/mM when the vertex potentials were set at –0.3 V and –0.4 V, respectively.

In order to elucidate the convection- and potential-dependent Q/Q_0 drop, effective coverage of I^- from Eq. 5 was analyzed under various conditions. (Figure 3.6) As shown in Figure 3.6(a), the effective coverage gradually increased at all potential ranges when elevating C_I. Notably, two peaks were formed at –0.15 V and 0.015 V, the positions of which shifted to a negative direction when increasing C_I. This indicates that at least two

chemical forms were involved in the suppression of the Cu reduction. The peak at 0.015 V was assumed to be related with I^- itself, while the peak at –0.15 V might have originated from the formation of CuI film on cathode surface. The electrochemical reduction of CuI can be expressed as shown at Eq. 9.

$$CuI + e \rightleftharpoons Cu + I^-, E^0 = -0.396 \text{ V (vs. Ag/AgCl [3 M KCl])} \quad \text{(Eq. 9)}$$

The reduction potential of CuI is computed by Eq. 10.

$$E_{Cu/CuI} = -0.396 - 0.059 \log C_I \text{ (vs. Ag/AgCl [3 M KCl])} \quad \text{(Eq. 10)}$$

Based on this calculation, the reduction of CuI begins at between –0.094 V (C_I = 7.55 μM) to –0.144 V (C_I = 53.3 μM), which was slightly higher than in our experimental results. The discrepancy between the peak potential and the reduction potential of CuI is related to the kinetic delay for the CuI reduction. As presented in Figure 3.6(b), a lower scan rate at which a broader interval for the CuI reduction is provided, shifted the peak from –0.169 V to –0.162 V, which is closer to the thermodynamic reduction potential of CuI (–0.152 V). The effect of electrodes' rotating speeds was also examined as presented in Figure 3.6(c). A diminished rotating speed resulted in a lower effective coverage in all potential ranges and the shift of the CuI reduction peak to the positive direction which

indicates that the C_I near the cathode surface is convection-dependent, so that a high rotating speed is required to enhance the suppression effect of I^-.

Figure 3.7 presents the schematic diagram of the procedure of CVS analysis. In the first step, the cyclic voltammogram of the base solution was obtained and the stripping charge (Q_0) was recorded. Next, the automatic dosing system dosed 1 mL of the standard solution and then CVS assessed the stripping charge (Q). This dosing procedure was repeated 8 times and then the responsive curve was made. In further determination process, the assessment of the stripping charge of the base solution was processed. Then, a target solution (3 mL) was added manually, the stripping charge of the target solution (Q_t) was calculated, and the Q_t/Q_0 was interpolated into the responsive curve for the determination by using Eq. 6.

The rotating speed with high analytical response (fast Q/Q_0 decrease with increasing I^- concentration) was adopted for further analysis. In choosing vertex potential, the intensity of stripping charge was considered because the small amount of deposited Cu at –0.1 V of the vertex potential leads to low resolution in determining concentration. Using the Q/Q_0 plot obtained with 2,000 rpm and –0.2 V of the vertex potential as the calibration curve (Figure 3.8(a)), the C_I in the target solutions with known C_I was

determined (Figure 3.8(b) and Figure 3.8(c)). Figure 3.8(b) shows that the determined C_I was well-matched to the real- C_I. The reliability of this method was also tested using various target solutions containing the same C_I of 250 μM, but different concentrations of the accelerator and suppressor. As shown in Figure 3.8(c), the determined C_Is were almost 250 μM, irrespective of accelerator and suppressor contents, which confirmed the reliability of this method under real solution conditions. An optimized RC-CVS was applied to monitor the TSV filling solution. TSV was well filled with metallic copper in case of the fresh TSV filling solution, as shown in Figure 3.9(a). However, the aged Cu acidic plating solution, which had been operated at 1 mA/cm^2 for 4,400 s, resulted in a void formation of the filling feature as depicted in Figure 3.9(b). The determined C_I of the aged solution showed 255 μM with optimized RC-CVS, and therefore, 145 μM of NH_4I was supplied to the aged Cu acidic plating solution. The TSV filling was performed with this refreshed solution (C_I = 402 μM). As shown in Figure 3.9(c), the filling performance recovered to its initial state. Consequently, the optimized condition for RC-CVS to monitor C_I was obtained under the assumption that CuI acted as a key inhibitor when a strong convection was applied. This method could be employed to monitor the C_I in the Cu plating solution for TSV filling.

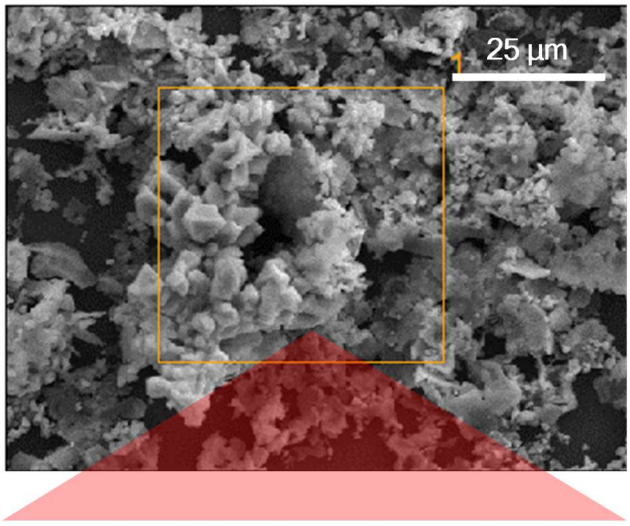

Element	Cu	I	C	O	Si
At%	**28.6**	**30.3**	8.6	15.7	16.8

Figure 3.1. FE-SEM image and EDS results of white particles formed on the cathode during Cu electrodeposition in VMS with the addition of 400 µM NH_4I.

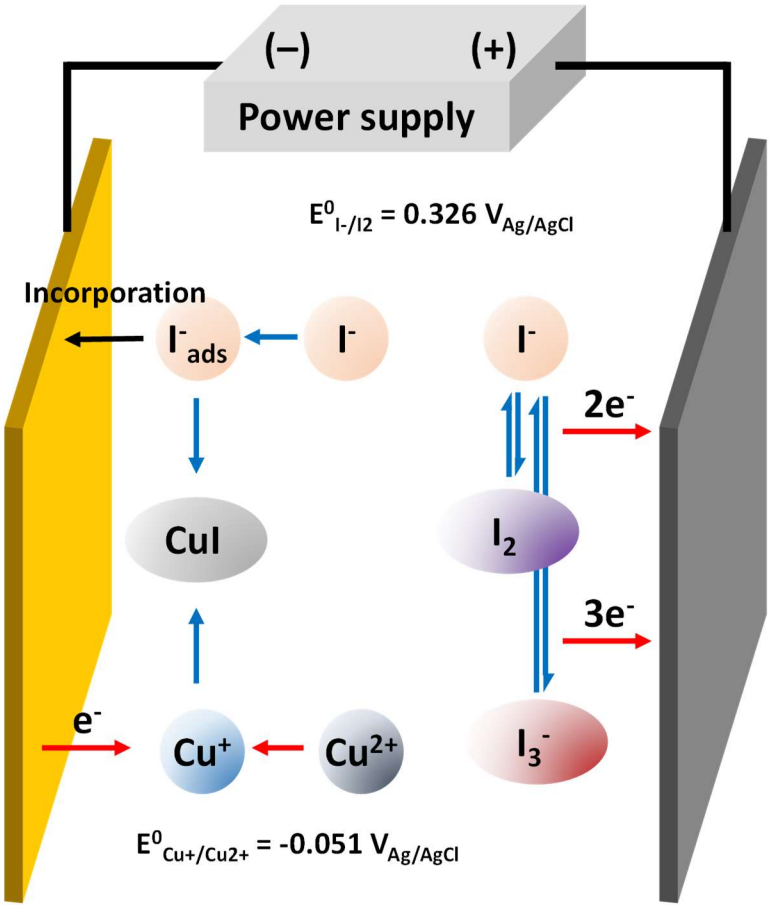

Figure 3.2. Schematic diagram of possible I^- consumption process.

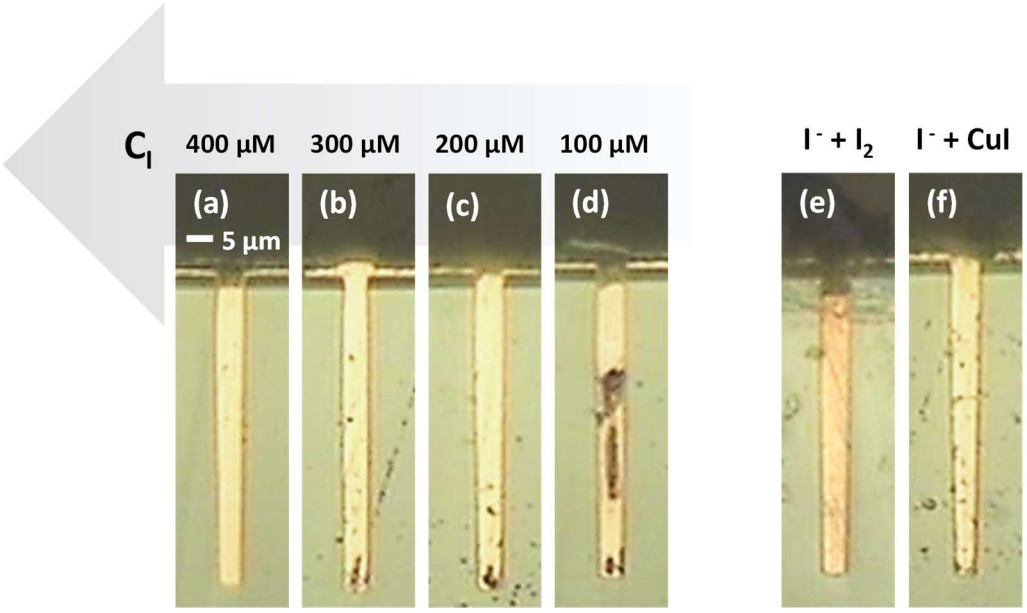

Figure 3.3. The cross-sectional optical microscope images of via-filling profiles deposited with (a) C_I = 400 μM, (b) C_I = 300 μM, (c) C_I = 200 μM, (d) C_I = 100 μM, (e) C_I = 400 μM and C_{I_2} = 800 μM, and (f) C_I = 400 μM and C_{CuI} = 800 μM. The TSV filling solution except I^-, I_2, and CuI was composed of VMS, 10 μM SPS, and 50 μM EPE.

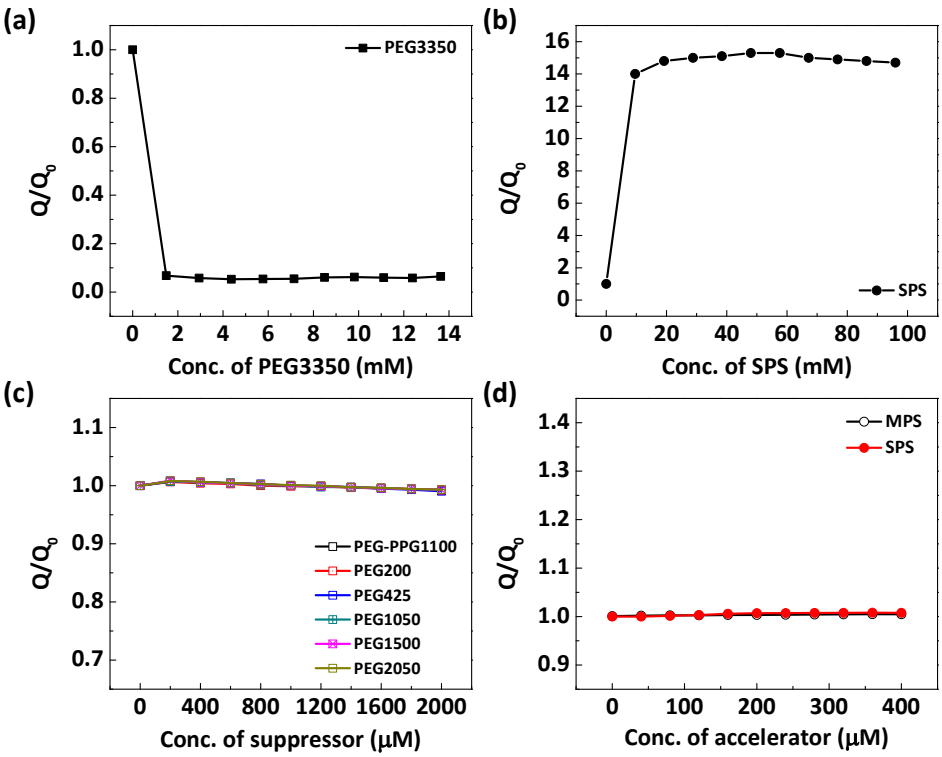

Figure 3.4. Q/Q_0 plot with the addition of (a) PEG3350 and (b) SPS into the VMS and the excluding effect of the base solution consisting of VMS, 2.88 mM PEG3350, and 19.2 mM SPS in the presence of various (c) suppressor and (d) accelerator species.

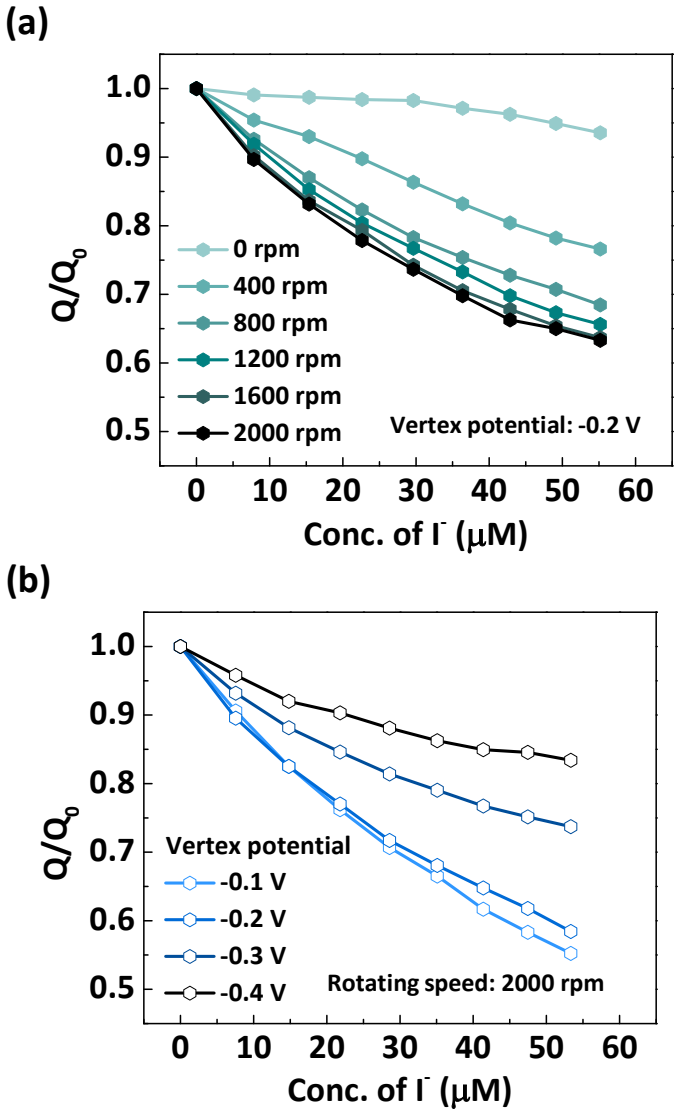

Figure 3.5. Q/Q_0 plot as a function of C_I in the base solution with various (a) rotating speeds of electrode and (b) the vertex potentials.

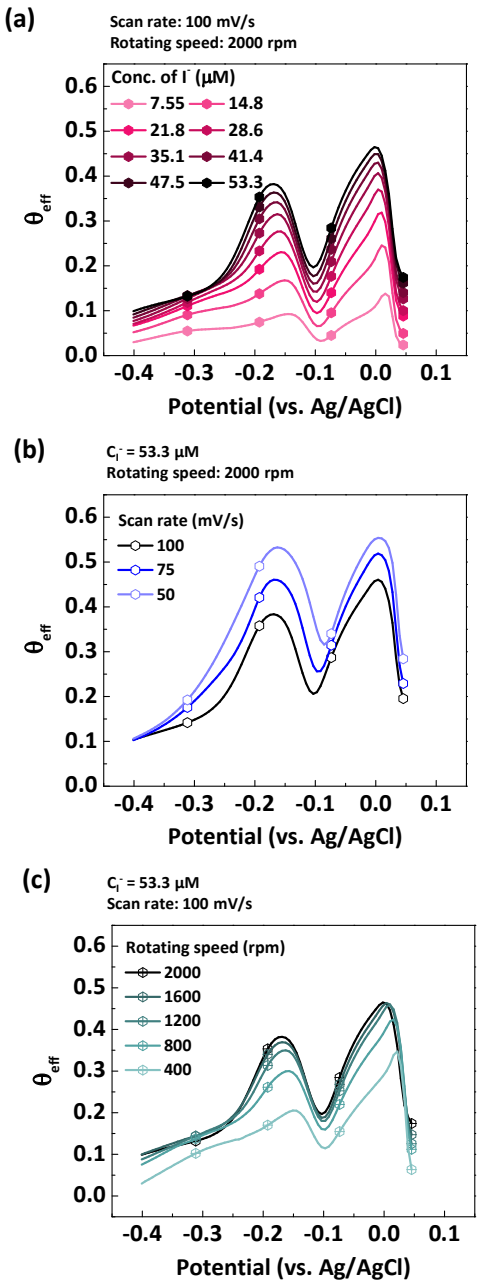

Figure 3.6. Effective coverage determined with Eq. 5 with various (a) C_I in the base solution, (b) scan rates, and (c) rotating speeds of electrode.

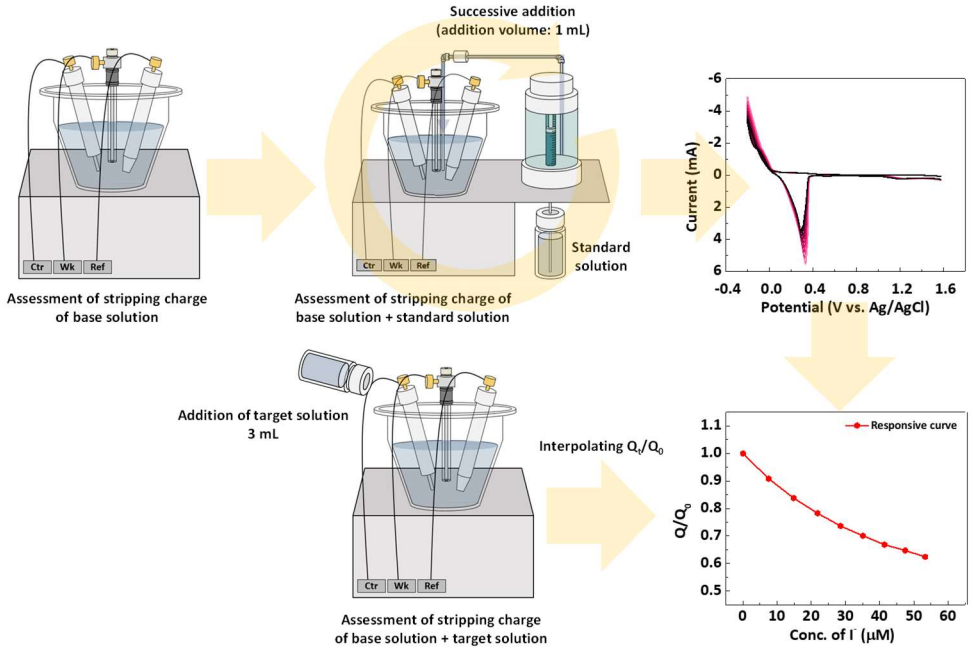

Figure 3.7. Schematic diagram of RC-CVS analysis.

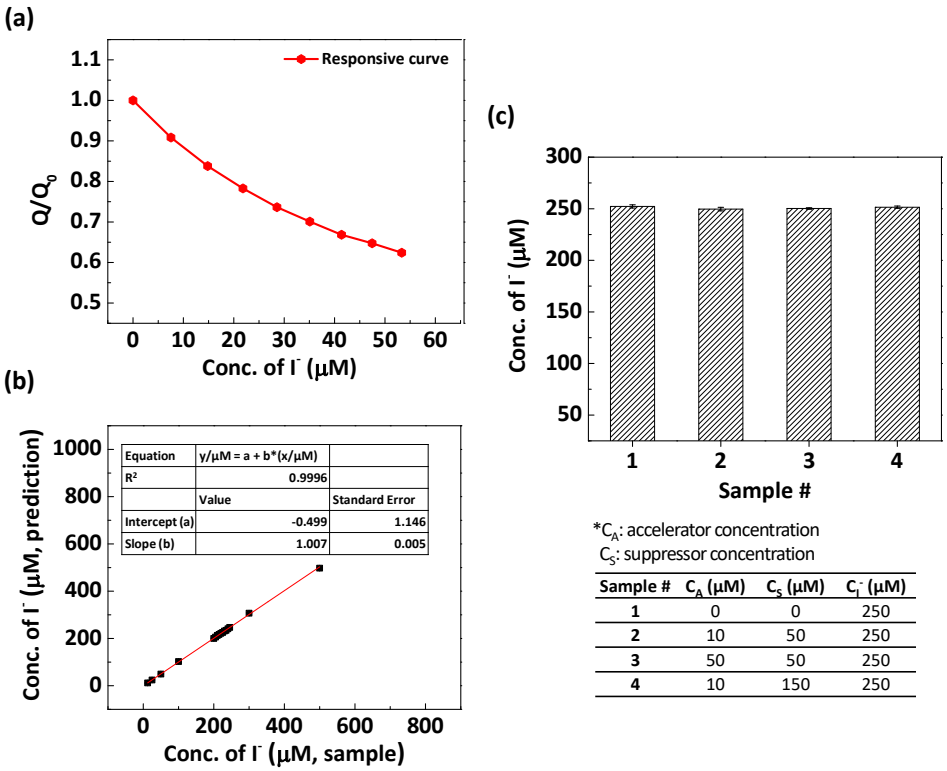

Sample #	C_A (μM)	C_S (μM)	C_I^- (μM)
1	0	0	250
2	10	50	250
3	50	50	250
4	10	150	250

Figure 3.8. (a) Q/Q_0 plots as a function of C_I in the base solution. The responsive curve is used for the determination of C_I in various target solutions. Real- and measured-C_I from the RC-CVS method (b) at fixed C_A (10 μM) and C_S (50 μM). Measured C_I at various C_A and C_S is also shown in (c). The target solution also contained VMS.

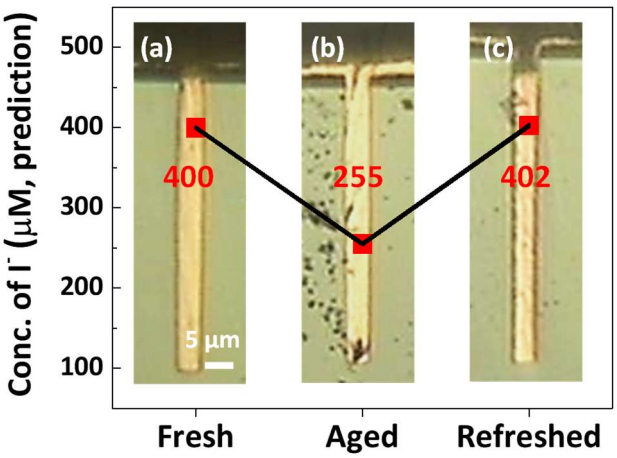

Figure 3.9. The cross-sectional optical microscope images of via-filling profiles deposited with (a) fresh Cu acidic plating solution, (b) the aged solution, and (c) the refreshed solution with the supplement of I^-. The measured C_I from RC-CVS analysis is also shown. The electrolytes for TSV filling solution also contained VMS, 10 μM SPS, and 50 μM EPE.

3.2 Selective determination of EPE concentration irrespective of SPS

3.2.1. Effect of SPS on the monitoring of EPE concentration and excluding effect of I^- for the action of SPS

Figure 3.10 reveals the Q/Q_0 plots as a function of C_S in the CVS bath with various C_A, simulating the effect of interference by SPS. The Q/Q_0 plots reveal that an extremely low concentration of SPS affected the value of Q/Q_0 at the same C_S. The C_S were determined by comparing the addition volume when the evaluation value ($Q/Q_0 = 0.7$) was interpolated in each Q/Q_0 plot, and an error of up to 19 μM was observed when using SPS-free solution as a standard. SPS increases the Cu plating rate as an accelerator by replacing the pre-adsorbed suppressor-Cu^+-Cl^- barrier. When EPE is added into the SPS-containing solution, it shows a stronger deceleration effect than in the additive-free VMS, and thus Q/Q_0 decreased faster than that in the SPS-free condition. The selective determination of C_S in a two-additive Cu plating solution via DT-CVS seemed hardly achievable, and a revised method was necessary to increase the selectivity of C_S measurement through eliminating the accelerating effect of SPS.

In order to deactivate the impact of SPS, I^- was used as a pretreatment. According to the literature, I^- was more strongly adsorbed on Pt surface than was Cl^-. Furthermore,

the passivation layer formed from PAG-Cu^{+}-X^{-} (X^{-}: halide ion) has characteristics that are dependent on the type of halide. Chemisorbed Cl^{-} on Cu substrate retains its negative charge due to its high electronegativity with relatively high solubility of CuX, which results in low stability in the disruption of the passivation layer formed with PAG by SPS-mediated breakdown. In contrast to Cl^{-}, Br^{-} has similar Cu-X bond length to CuCl despite its larger size than Cl^{-}, due to its large polarizability with low solubility of CuX, which leads to strong and stable PAG-Cu^{+}-Br^{-} that is resistive to SPS-mediated breakdown.[81] I^{-} has lower electronegativity and much lower solubility of CuI, compared with those of Br^{-}, and considering the same analogy, I^{-} could form much more stable PAG-Cu^{+}-I^{-} layer that was highly resistive to the displacement by SPS, and could be applied to the determination of C_S in the two-additive Cu electroplating samples.

In Figure 3.11(a), the addition of SPS to the EPE-containing electrolyte made the onset of Cu electroplating earlier, and significantly increased the deposition rate in the forward sweep, compared to the EPE-only condition. This indicated the SPS-mediated breakdown of the suppressor layer, allowing a larger current by its anti-suppressing mechanism than the current in the additive-free condition. Therefore, the presence of SPS could interfere with the selective C_S measurement, and it was necessary to eliminate this effect. The addition of 400 μM I^{-} shown in Figure 3.11(b) slowed down the

deposition of Cu compared to the EPE-only condition in Figure 3.11(a), and allowed effective Cu plating to proceed at a more negative potential, because of the much more stable EPE-Cu^{+}-I^{-} layer, as well as its own suppression effect. Even though excess SPS was added, the layer was not rapidly disrupted, and effectively slowed the Cu plating to a negative potential, compared to the EPE-SPS case. In the reverse sweep after vertex potential, the EPE-I^{-} case and EPE-SPS-I^{-} case showed the same relaxation current behavior, which could be explained by the dominant interaction between EPE and I^{-}.

3.2.2. Optimization of the formation of EPE-Cu^{+}-I^{-} layer and its application to selective CVS analysis for EPE concentration

The stability of the suppressor-passivating layer during the CV analysis of Cu electroplating on Pt cathode was affected by the scan rate and vertex. This is because the EPE-Cu^{+}-X^{-} layer needs Cu^{+} ion to be formed, and metallic Cu where it adsorbed, both of which needed the reduction of Cu^{2+}. Figure 3.12 shows that the voltammetric behavior of EPE-SPS-I^{-} in the forward sweep changed almost exactly as in the EPE-I^{-} case by lowering the scan rate with vertex of –0.35 V, which means sufficient amount of Cu^{+} to maximize the formation of EPE-Cu^{+}-I^{-} layer with the formation of CuI in the deposition

process, thereby completely removing the interference by SPS. Therefore, the EPE-I^- behavior could be optimized by controlling the electrochemical variables. Under certain conditions, the EPE-I^- system was not affected by SPS.

Effective coverage defined as Eq. 11, which means the strength of the suppressing agent at a certain potential, was introduced to analyze the results based on the current in Figure 3.13(a):

$$\theta_{\mathrm{eff,sup}} = 1 - i_{\mathrm{add}}/i_{\mathrm{none}} \qquad \text{(Eq. 11)}$$

where, i_{add} is the plating current with additives, and i_{none} is the plating current without an additive. In the EPE-only case shown in Figure 3.13(b), the effective coverage was maintained at around 0.85 at the initial stage of forward scan between 0.05 and –0.15 V, because of EPE adsorption. As Cu plating started, the suppressing layer was disrupted with the start of Cu^{2+} reduction, and the convergence of effective coverage to zero could confirm this. In the reverse sweep, the effective coverage was not recovered as much as that of the forward scan, because of the delay for re-adsorption of EPE, which is also the main reason for hysteresis in cyclic voltammograms. For the EPE-SPS system, the effective coverage decreased sharply to near zero, and even became negative, owing to the catalytic acceleration of Cu^{2+} reduction by SPS. This could be interpreted as the

acceleration by SPS, via both mechanisms of anti-suppression and catalytic acceleration. The small difference between effective coverage in forward and reverse scans could explain the decrease in hysteresis. In the case of the EPE-SPS-I^- system, the effective coverage in the forward scan was restored to its original level, and the effective coverage in the reverse scan was also similar to that in the forward scan.

Consequently, the EPE-I^- combination was necessary for maintaining the stripping charge, even in the interference by the accelerator. In this SPS-excluding condition, additional peaks were observed in the stripping region (the region where the plated Cu is oxidized to Cu^{2+} ion), as shown in Figure 3.14(a). These peaks could be assigned to the oxidation of CuI ($CuI \rightarrow Cu^{2+} + I^- + e$, $E = 0.454\ V_{Ag/AgCl}$, considering 400 μM of I^- with unit activity coefficient), supported by the peak potential range. The intensity of these peaks depended on the amount of CuI formed during the deposition process, which was supported by the data in Figure 3.14(b). The ratio between the charge of Cu stripping and CuI oxidation was dependent on the scan rate. When the slower scan rate was applied, the ratio of CuI formed during the analysis to the deposited Cu increased. Considering the accelerating effect of SPS was removed at slow scan rate, it could be concluded that the greater the formation of CuI and the greater the CuI deposition relative to Cu, the

weaker the action of SPS under the EPE-I^- condition. The amount of CuI and the interaction with EPE inhibited the accelerating effect of SPS by forming stable EPE-Cu^+-I^- layer in negative vertex potential and slow scan rate.

Au wafer was attached on the teflon RDE to simulate the analytic environment of CVS analysis. The electric contact was made using Al foil shielded by the chemical-protective waterproof tape. The composition of the surface of deposits obtained from the CV method in the Cu plating solution on Au wafer with various scan rates is summarized in Figure 3.15(a), indicating slower scan rate exhibited higher content of iodine (I). Figure 3.15(a) also shows the SEM and EDS mapping of the sample deposited with 20 mV/s. Bumps with particles where Cu and I were uniformly distributed were observed along the surface. In Figure 3.15(c), the X-ray diffraction (XRD) pattern reveals two peaks at 2θ = 25.6 deg and 52.5 deg, which could be assigned as (111) and (222) of γ phase of CuI, respectively. X-ray photoelectron spectroscopy (XPS) in Figure 3.15(d) further confirm the peaks of CuI at 619.3 eV (I $3d_{5/2}$) and 630.8 eV (I $3d_{3/2}$) without any satellite peak, revealing that most of I was present on the surface in the state of CuI. Therefore, during the CVS analysis, CuI is uniformly formed on the electrode surface, and this affects the interaction of the deposit with PAG.

Figure 3.16 summarizes the schematic diagram of the acting mechanism of I^- on improving detection accuracy by excluding the effect of SPS. Without I^-, the Cu deposit is formed on Pt electrode during CVS analysis. On the electrode, Cu, Cl^-, and EPE are involved in to construct suppressor layer and slow down further Cu electroplating. This suppressor layer is easily broken by SPS due to the catalytic effect of the accelerator on Cu electroplating. However, with I^-, CuI particles with Cu bumps are formed on Pt electrode, which is confirmed by the surface characterization in Figure 3.15. This surface state has advantage on forming robust PAG-Cu^+-I^- suppressor layer and this layer reveals strong resistance to the displacement and catalytic effect by SPS, which corresponds to enhancing accuracy in determining C_S even with the interference of SPS.

It was hypothesized that the formation of large amounts of CuI and the interaction with EPE during CVS analysis could prevent the disruption of EPE-Cu^+-I^- layer by SPS. Figure 3.17 shows that the potential for onset of the deposition did not change even though I^- was added, so the suppressor predominantly determined the onset of the Cu deposition. The difference resulting from I^- addition was the decrease in the current in the deposition region, which could be interpreted as the more difficult inner-diffusion of Cu^{2+}/Cu^+ ion into the inhibition layer due to the CuI and the interaction with EPE, compared to CuCl with EPE. When I^- alone was added, the acceleration by SPS was

hardly observed, because the stable, hydrophobic, and covalent-bonding CuI layer was not destroyed by SPS. The combination of the effect of CuI and EPE-Cu^{+}-I^{-} layer synergistically inhibited the SPS-mediated breakdown of the passivation layer.

Comparing Figure 3.18(a) and Figure 3.18(b), increase in C_S made the onset potential of Cu more negative in the suppressor-only case, while both the Cu depositions started at 0.05 V with the addition of SPS. Increase in CS builds the stronger inhibition layer, but the layer is easily disrupted by 10 μM of SPS. However, with I^{-} as in Figure 3.18(c) and Figure 3.18(d), even the addition of SPS could not start the Cu electroplating earlier, which means that a stronger passivation layer was formed, compared with the suppressor-only case. In the reverse sweep, the current was not interfered with by SPS, which reveals there was no intervention of the accelerator in Cu electroplating in the deposition region. It is apparent that the current-potential behavior was largely influenced by the EPE-Cu^{+}-I^{-} layer formation and disruption by permeation of Cu^{2+}/Cu^{+} ion, rather than the breakdown by SPS due to competitive adsorption.

The modified CVS analysis is described as follows: (1) The standard Q/Q_0 curve is obtained with the same procedure used in DT-CVS analysis, except for the base solution of VMS with the added 400 μM I^{-}. Also, 400 μM of I^{-} is added into the standard solution,

which contains a known amount of suppressor (C_S = 50 μM). (2) Fresh CVS bath is prepared. The stripping charge (Q_0) of the base solution is evaluated, and then a specific volume (3 mL, in the determination step) of a target solution is added to calculate the stripping charge (Q), and evaluate the Q/Q_0 value. The Q/Q_0 value is interpolated in the response curve to determine the concentration of suppressor in the target solution.

Figure 3.19(a) shows the Q/Q_0 plots as a function of C_S in the CVS bath. The response curves were obtained using the aforementioned process, and the Cu electroplating solutions used for this response curve contained various concentrations of SPS from 0 to 100 μM. The Q/Q_0 plots showed the same response to the C_S in the CVS bath, irrespective of the C_A in the electroplating solution, which means the modified methods could exclude the effect of SPS. Various target solutions were tested using this method, and the determination of C_S in the solutions showed small errors with high linearity (R^2 = 0.9986 in Figure 3.19(b)). Our devised method successfully monitored a wide range of C_S in various target solutions, irrespective of C_A.

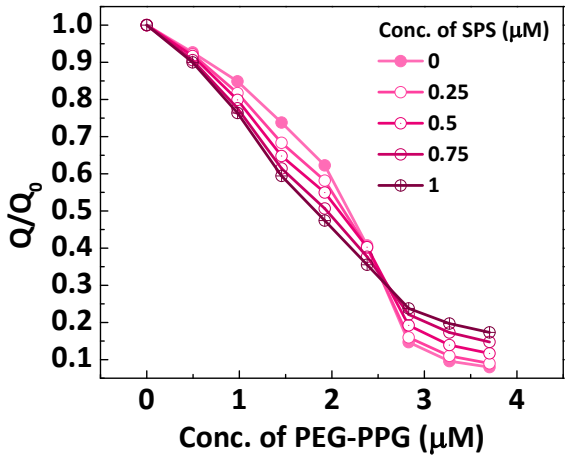

*C_A: concentration of SPS
C_S: concentration of EPE

C_A (μM)	Determined C_S (μM)
0.25	54.5
0.5	59.2
0.75	65.3
1	69.0

Figure 3.10. Q/Q_0 plots with various C_A in VMS as a function of C_S and determined C_S with the interference of SPS at 0.7 evaluation value.

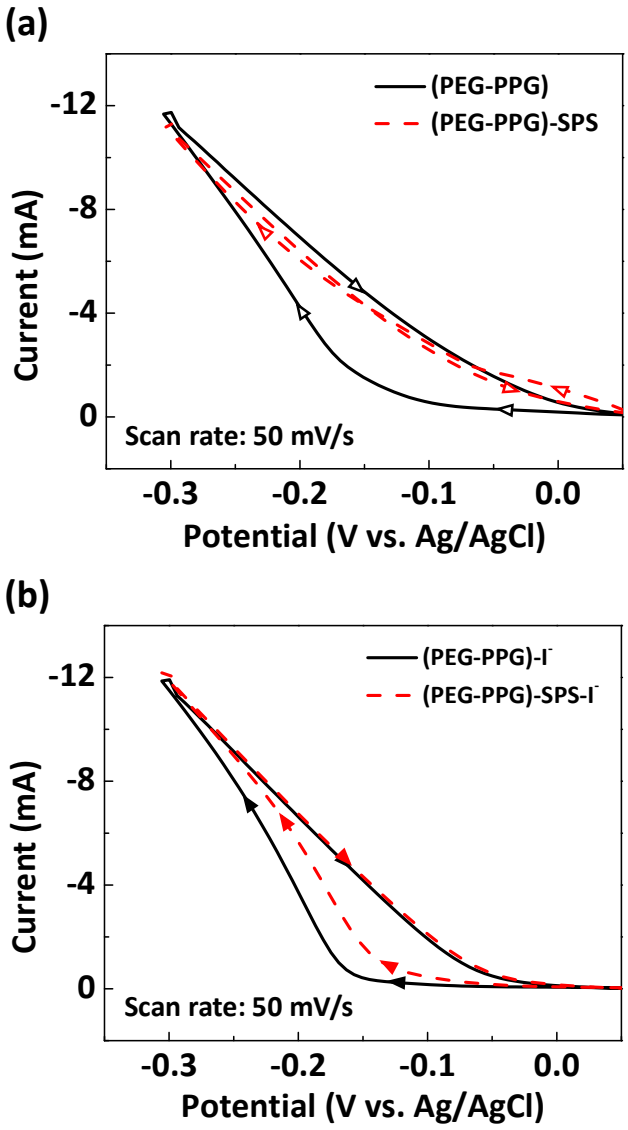

Figure 3.11. Cyclic voltammograms of Cu electroplating in deposition region with (a) EPE/EPE-SPS and (b) EPE-I^-/EPE-SPS-I^- (C_S = 2 μM, C_A = 10 μM, and C_I = 400 μM in VMS).

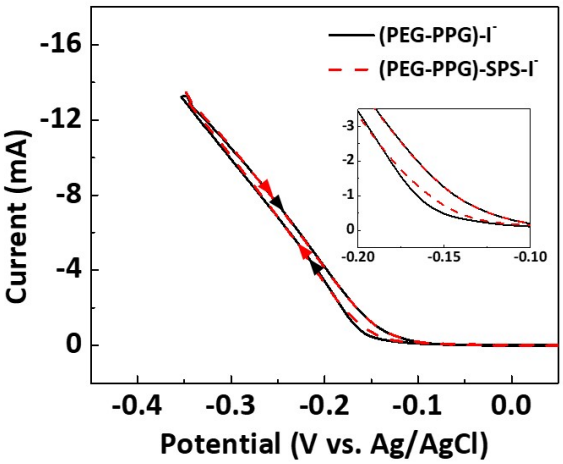

Figure 3.12. Cyclic voltammograms (vertex: –0.35 V, scan rate: 20 mV/s) EPE-I^-/EPE-SPS-I^- systems (C_S = 2 μM and C_I = 400 μM in VMS).

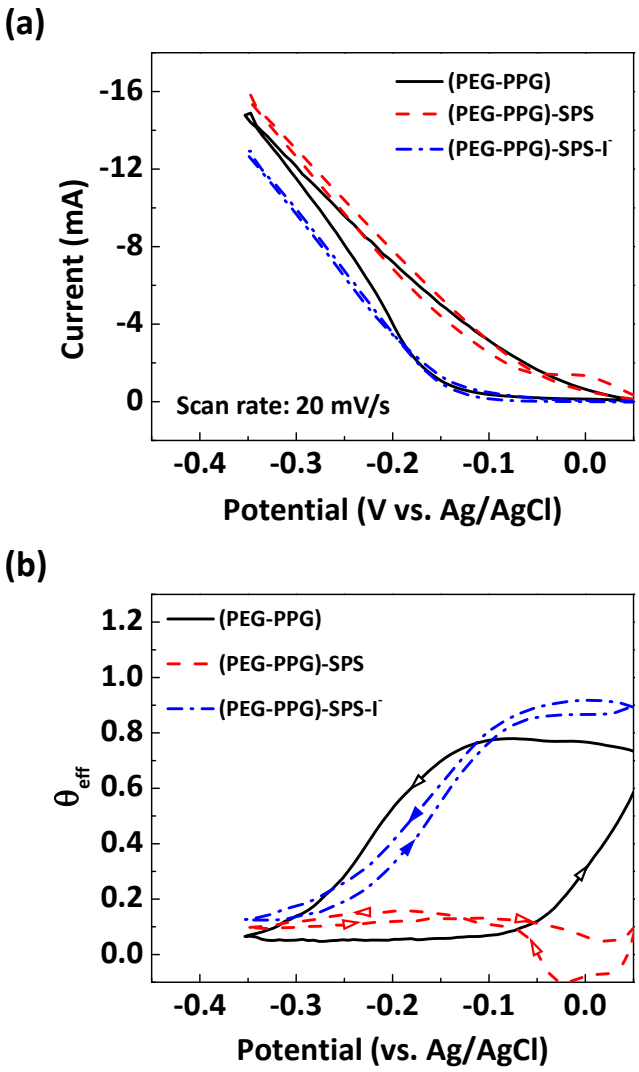

Figure 3.13. (a) The current-potential behavior of Cu electroplating and (b) effective coverage (Eq. 11) with EPE/EPE-I^-/EPE-SPS-I^- (C_S = 2 μM, C_A = 10 μM, and C_I = 400 μM in VMS).

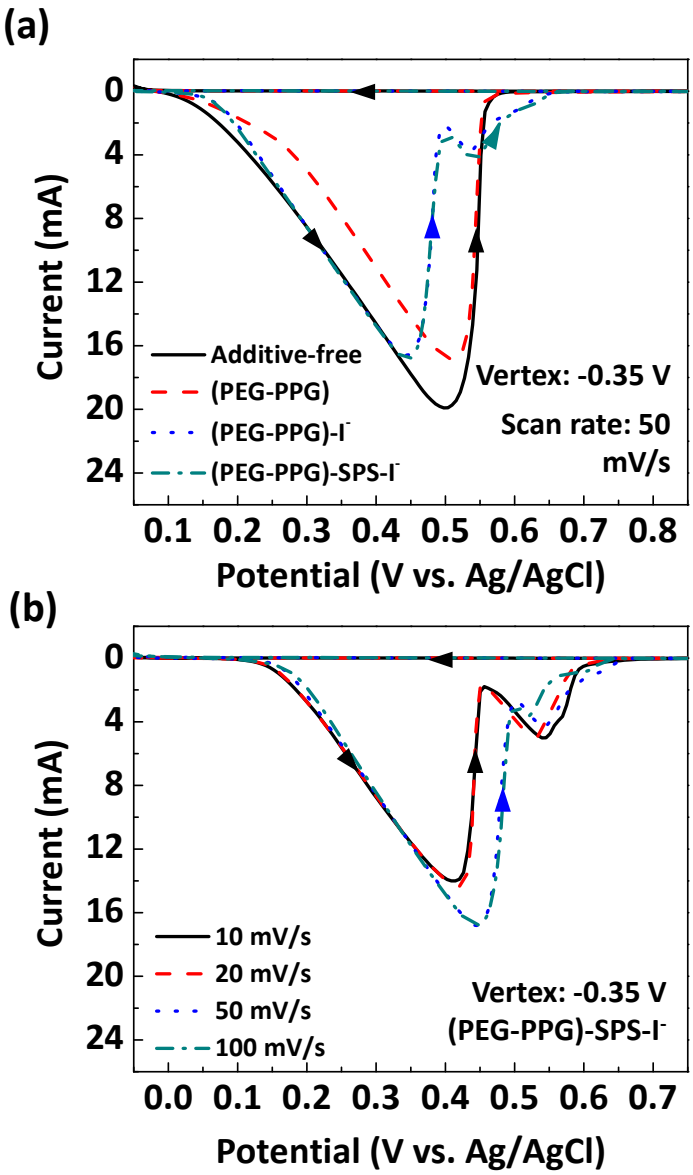

Figure 3.14. Current-potential behavior in stripping regions (a) with various combinations of additives, and (b) effect of the scan rate (C_S = 2 μM, C_A = 10 μM, and C_I = 400 μM in VMS).

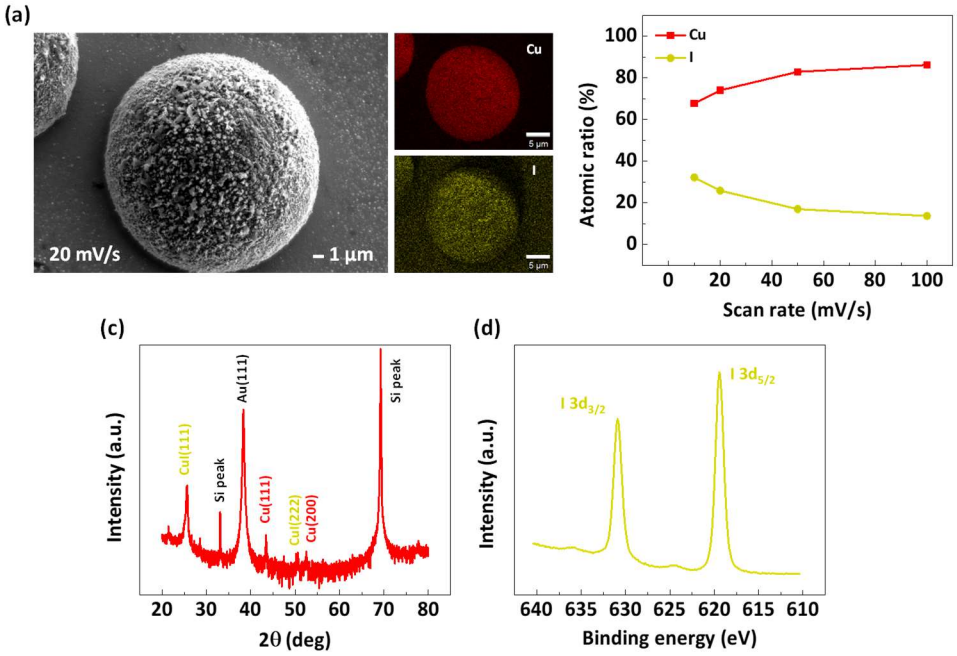

Figure 3.15. (a) Surface morphology and EDS mapping of Cu and I of the deposit with the scan rate of 20 mV/s confirmed by FE-SEM and atomic ratio of Cu and I as a function of scan rate. (b) XRD and (c) XPS spectrum of the same sample. The Cu electroplating solution contained VMS, 10 µM SPS, 2 µM EPE and 400 µM NH_4I.

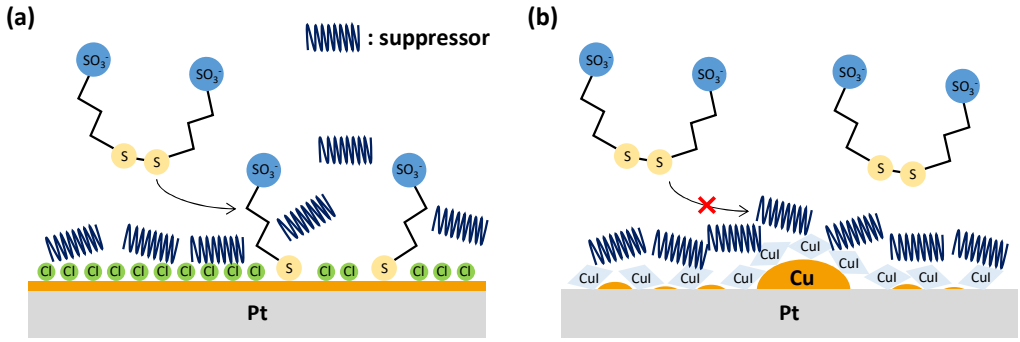

Figure 3.16. Schematic of the behavior of accelerator and suppressor (a) without and (b) with I^-.

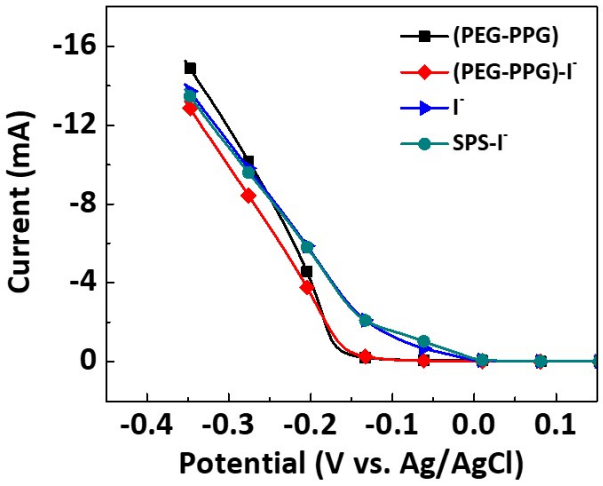

Figure 3.17. LSV in deposition region of EPE/EPE-I^-/I^- and SPS-I^- systems (C_S = 2 μM, C_A = 10 μM, and C_I = 400 μM in VMS).

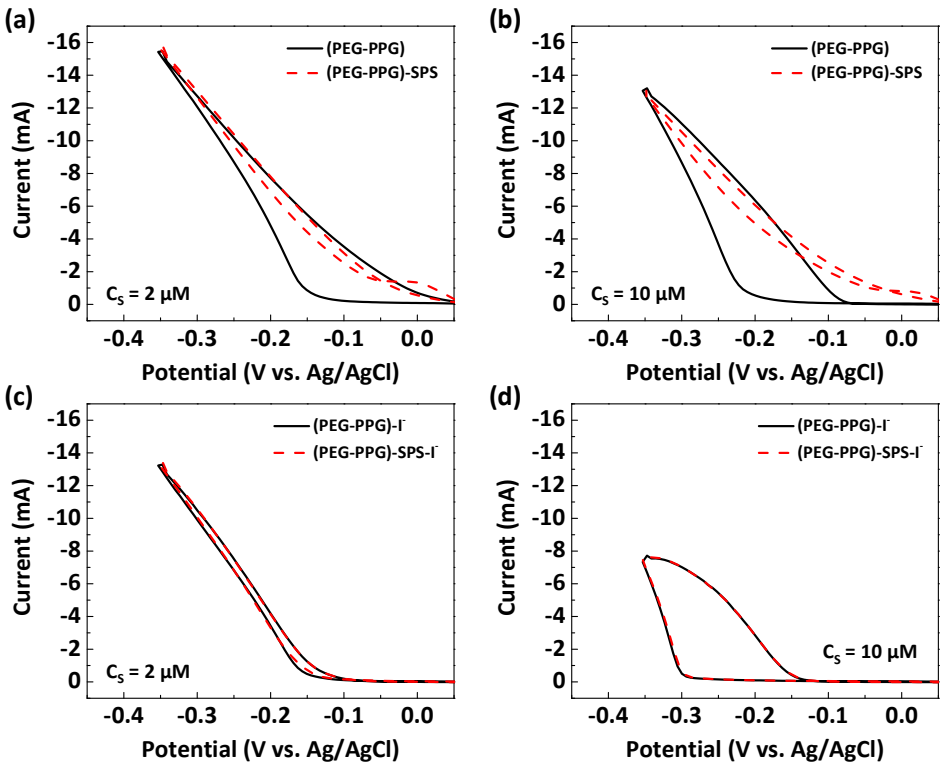

Figure 3.18. CV of EPE/EPE-SPS in (a) low C_S (2 µM), and (b) high C_S (10 µM) in VMS, and EPE-I^-/EPE-SPS-I^- in (c) low C_S (2 µM), and (d) high C_S (10 µM) in VMS.

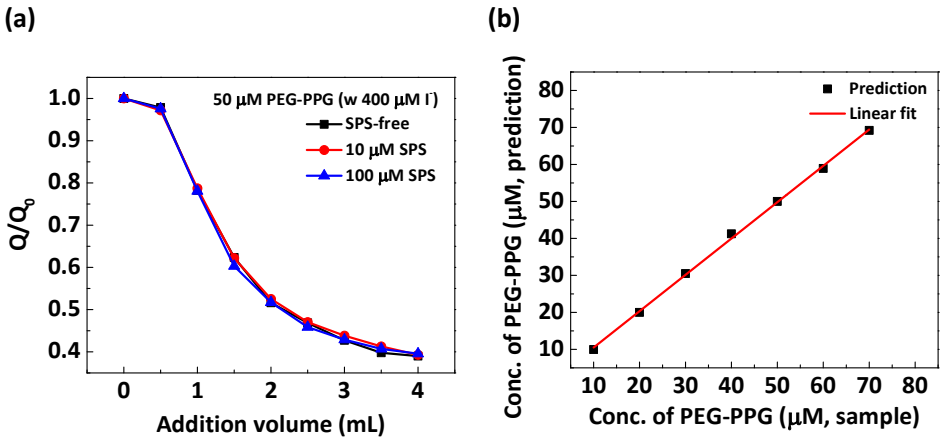

Equation	y/μM = a + b*(x/μM)	
R^2	0.9986	
	Value	Standard Error
Intercept (a)	0.861	0.791
Slope (b)	0.979	0.017

Figure 3.19. (a) Response curves (Q/Q_0 as a function of C_S) obtained from Cu electroplating solutions with C_S = 50 μM and C_A = 0, 10, and 100 μM in VMS, and (b) real and measured C_S from the modified method with various target solutions. The target solution also contained VMS and random amount of SPS.

3.3 Machine learning for monitoring the concentration PEG with various molecular weight

3.3.1. Prediction of concentration in PEG3350/Cl^- system using various machine learning algorithms

The results of predicting the concentration of each additive in PEG3350/Cl^- system using the k-NN algorithm are summarized in Figure 3.20. Figure 3.20(a) shows the performance of the model for the parameter, *n_neighbors*, and the smallest root mean square error (RMSE) was calculated when *n_neighbors* = 2. This optimized parameter was applied to predicting the test dataset. As in Figure 3.20(b) and Figure 3.20(c), the model based on k-NN algorithm showed R^2 = 0.9907 and 0.9809, respectively, for determining PEG3350 and Cl^- concentration, which was impossible in conventional CVS analysis. Although the k-NN algorithm suggested the feasibility of electrochemical analysis using machine learning, it takes long time to predict a data point with high dimensions such as CV analysis.

When the linear model was used, the prediction performance of PEG3350 was slightly improved (Figure 3.21(a)), but the performance of determining Cl^- concentration became poorer (Figure 3.21(b)) than that of k-NN. The advantage of the linear model is

visualization of the weights, which is multiplied by the current, at each potential, and by normalizing the absolute value of each weight so that the sum of the absolute weight becomes 1, the visualizations for the forward scan and the backward scan can be shown for each additive. As shown in Figures 3.21, the normalized absolute weights in deposition region for the forward scan (Figure 3.21(c) and Figure 3.21(e)) is larger than those for the backward scan (Figure 3.21(d) and Figure 3.21(g)). In CV analysis for PEG3350/Cl^- additive composition in Cu electrodeposition system, PEG and Cl^- synergistically inhibit Cu electrodeposition during the forward scan, and after the deposition starts, PEG-Cl inhibition layer is disrupted and PEG is desorbed from the electrode. When the backward scan starts, the inhibition layer cannot recover even the sweeping potential approaches to the onset of Cu electrodeposition due to the slower kinetics of the large MW polymer. Therefore, the relaxation current in the deposition region during the backward scan is usually dominated by the Cu^{2+} reduction without the action of the additives. This could explain the larger absolute weights within the deposition region in forward scan. The evolution of the normalized absolute weights within the stripping region during the backward scan means the change in the stripping peak also assists determining the concentrations of the additives. The linear model provides the insights of the behavior of the additives from the weight-visualization, but

it could not yield prediction precisely due to the nonlinear response of the current from the change in additive concentration.

In the prediction model using the random forest, the predictive performance for both PEG3350 (Figure 3.22(a)) and Cl^- (Figure 3.22(b)) was slightly inferior to those of other algorithms, which is interpreted as the model exhibits overfitting to the training dataset due to the absence of pre-pruning setting during the model training process. Like the linear model, the random forest model can also plot the feature importance in the forward scan and backward scan according to the potential, as shown in Figure 3.22(c) and Figure 3.22(d). In particular, the feature importance around 1.4 $V_{Ag/AgCl}$ in the backward scan was strong, which appears to be due to the chloride oxidation (Cl_2 (g) + 2e ⇌ 2Cl^-), and it can be interpreted that the current at the region helps to determine the concentration of Cl^-. The random forest can also trace back the electrochemical reaction, which is important for additive concentration analysis through the reverse engineering of the model, but the real-time performance decreases as the number of trees increases.

3.3.2. Prediction of concentration in PEG3350/Cl^- system using artificial neural network

Using the combination of PEG3350 and Cl^-, which are active in CV analysis, the performance of the neural network-based model was verified in a simple chemical composition system. PEG3350 and Cl^- synergistically interact to form inhibition layer for Cu^{2+} reduction, decreasing the intensity of signal (current) in the deposition and stripping region with increase in each concentration, as in Figure 3.23(a) and Figure 3.23(b). After labeling the CV results at various concentration combinations of PEG3350 and Cl^- as concentration vectors, data preprocessing was performed to reduce the bias of the feature value when training the model. As shown in Figure 3.23(c) and Figure 3.23(d), the observed current at each potential was standardized with zero-centered and unit standard deviation. 80% of the dataset was divided into the training dataset, and 20% into the test dataset, and each was used for leaning and evaluation. The neural network model contains one hidden layer, and the size of the hidden layer, the hyper parameter, was determined through a cross-validation process using training dataset. The training dataset was split into 5 folds, and each fold was used as validation, and the hyper parameter was determined through the average of the root mean square error (RMSE). As shown in Figure 3.24(a), when the layer size is more than 20, the RMSE determined from the prediction of the model is saturated, and the optimal value is determined at 67. The results of predicting the concentration of PEG3350 (Figure 3.24(b)) and Cl^- (Figure

3.24(c)) at the optimized hyper parameter. The model trained through concentration-labeled analysis results observed in simple electrochemical systems was appropriate to predict chemical information from unknown electrochemical analysis results, and for PEG3350 and Cl^-, R^2 was higher than 0.99, showing high accuracy.

3.3.3. Accuracy improvement for prediction of concentration in PEG200/PEG1500/PEG3350/Cl^- system

In a system composed of CV-active PEG3350, PEG1500, Cl^-, and CV-inactive PEG200, the neural network model was trained in the same manner as the above method. As shown in Figure 3.25(a), a neural network model with current as input and concentration as output was built, and the optimized size of the hidden layer was 87. Figure 3.25(b) to Figure 3.25(e) show the results of predicting the concentration of PEG3350, PEG1500, PEG200, and Cl^-. Unlike a simple system composed of only PEG3350 and Cl^-, the prediction performance for PEG3350 slightly decreased to R^2 = 0.9867, and it was observed that the lower the molecular weight of PEG, the inferior the prediction performance. On the other hand, the prediction of concentration for Cl^- was still reasonable. The deterioration of prediction performance in PEG3350 concentration

is ascribable to the competition for adsorption with other PEGs with lower MW. Since the amount of Cl^-, which serves as a mediator for adsorption of PEG on the electrode surface, is limited, the adsorption of PEG becomes more difficult compared to that in the PEG3350/Cl^- system, reducing CV activity of PEG3350 (Figure 3.26(c)). This also applies to PEG1500 and PEG200 (Figure 3.26(a) and Figure 3.26(b)). In addition, even if the mass concentration of PEG is controlled to have the same number of monomer units, low molecular weight PEG (i.e., PEG200) rarely inhibit the Cu electrochemical deposition due to its weak adsorption on Cl^--saturated surface, decreasing CV activity of the PEG. Therefore, as the molecular weight of PEG decreases, the performance of the model decreases. On the other hand, in the case of Cl^-, since it acts as an adsorption site for various PEGs, the higher the concentration in the complex PEGs system, the more effectively an inhibition layer against Cu electrochemical deposition could be formed with the PEGs, well shown in Figure 3.26(d). As a result, the CV activity of PEG decreases in the electrochemical analysis process due to the interference by the competition of adsorption between PEGs, occurring with limited Cl^- in the complex PEGs system, leading to difficulty in predicting each of the concentration of PEG.

Improvements to the prediction could be achieved by enhancing the CV activity of the PEGs and providing sufficient adsorption sites for the PEGs. One of the method to

increase the responsiveness of a PEG in CV analysis is to shift the switching potential to a more positive one. The inhibition layer formed by PEG and Cl^- increases the overpotential of Cu electrochemical deposition, however when sufficient energy to overcome this is applied, Cu electrochemical deposition occurs actively along with the desorption of PEG. Therefore, it is possible to improve the CV activity for each PEG by performing CV analysis to the switching potential where the inhibition layer could be maintained. In the case of PEG3350 and PEG1500 (Figure 3.27(b) and Figure 3.27(c)), the inhibition layer was effectively maintained when the switching potential was shifted from $-0.4\ V_{Ag/AgCl}$ to $-0.2\ V_{Ag/AgCl}$, resulting in a decreased Cu electrochemical deposition rate as a change in the stripping area ($Cu \rightarrow Cu^{2+} + 2e$) during the reverse sweep. This was clearly observed for Cl^- as shown in Figure 3.27(d). However, in the case of PEG200 (Figure 3.27(a)), the responsivess in CV did not improve even with the change in the switching potential, attributed by the inherent weak adsorption of PEG200. PEG with a low molecular weight (i.e., PEG200) could not form an effective inhibition layer against Cu electrochemical deposition no matter how high the concentration is, since the number of ethylene oxide groups in the polymer which could adsorb on Cl^- on the electrode surface is small. The introduction of halide ions other than Cl^- could

enhance the adsorption properties of low-molecular PEG, and when I^- was used as a pretreatment for the analyte, the CV response to the concentration of each PEG was improved (Figure 3.28). The responsiveness to PEG3350 and PEG1500 was also improved compared to the response in –0.4 $V_{Ag/AgCl}$ switching potential without the pretreatment.

The introduction of I^- affected Cu^+ formation and Cu stripping ($Cu \rightarrow Cu^{2+} + 2e$) in during the electrochemical analysis. As shown in Figure 3.29(a) to Figure 3.29(c), in the CV analysis where only Cu^{2+} reduction and Cu stripping were observed in I^--free condition, I^- pretreatment induced various electrochemical reactions involving Cu, Cu^+, and I^-. Basically, I^- inhibits Cu electrochemical deposition by increasing the overpotential for Cu^{2+} reduction, forming copper iodide (CuI) which is formed from the reaction between Cu^+ and I^- and acts as an insulating layer on the electrode surface (Figure 3.29(a)). The peak observed at –0.4 $V_{Ag/AgCl}$ during the forward potential sweep under I^--free condition is assigned Cu^{2+} reduction to Cu^+, which could be observed due to the low activity of Cu^+ when analyzing the Cu^{2+} electrolyte using a Pt electrode. The peak change with I^- concentration (Figure 3.29(b)) could be ascribable to the change in the activity of Cu^+ due to the reaction with I^-, which occurs at the first reduction step of

Cu^{2+} ($Cu^{2+} + e \rightarrow Cu^{+}$). Also, as the concentration of I^- increases, the peak observed near 0.48 $V_{Ag/AgCl}$ in the reverse sweep increases (Figure 3.29(c)) because the CuI is electrochemically oxidized ($CuI \rightarrow Cu^{2+} + e$) in the corresponding potential region. When PEG200 is added into the basis analyte pretreated with I^-, effective inhibition layer is formed compared to that with PEG200 and Cl^-, which is revealed by a decrease in the rate of Cu electrochemical deposition and a corresponding decrease in stripping charge as shown in Figure 3.29(d). PEG200 affects both the formation and oxidation of CuI, and it is revealed that the CV activity of PEG200 increases from the complex chemical/electrochemical reaction (Figure 3.29(e) and Figure 3.29(f)).

Using I^- as a pretreatment for improving the CV response of PEG, a new dataset was constructed and model optimization was performed in the same manner. The optimized hyper parameter is the layer size of 87, which is the same as the previous model without chemical/electrochemical control. As a result, the performance of concentration prediction was improved for all PEGs (Figure 3.30). R^2 especially improved from 0.9293 to 0.9949 for PEG200, which showed the largest error of measurement, and increased from 0.9791 to 0.9954 for PEG1500 and from 0.9867 to 0.9976 for PEG3350. Cl^- showed unchanged reasonable performance in predicting concentration (R^2 = 0.9997).

Consequently, through chemical control (introduction of I^- as a pretreatment agent) and electrochemical control (change in switching potential), the electrochemical response to the analysis of each species in a complex PEGs/Cl^- system was improved. The concentration of species could be predicted with more than a certain level of accuracy from the results of electrochemical analysis without having to perform appropriate pretreatment for each species or obtain a calibration curve for each species.

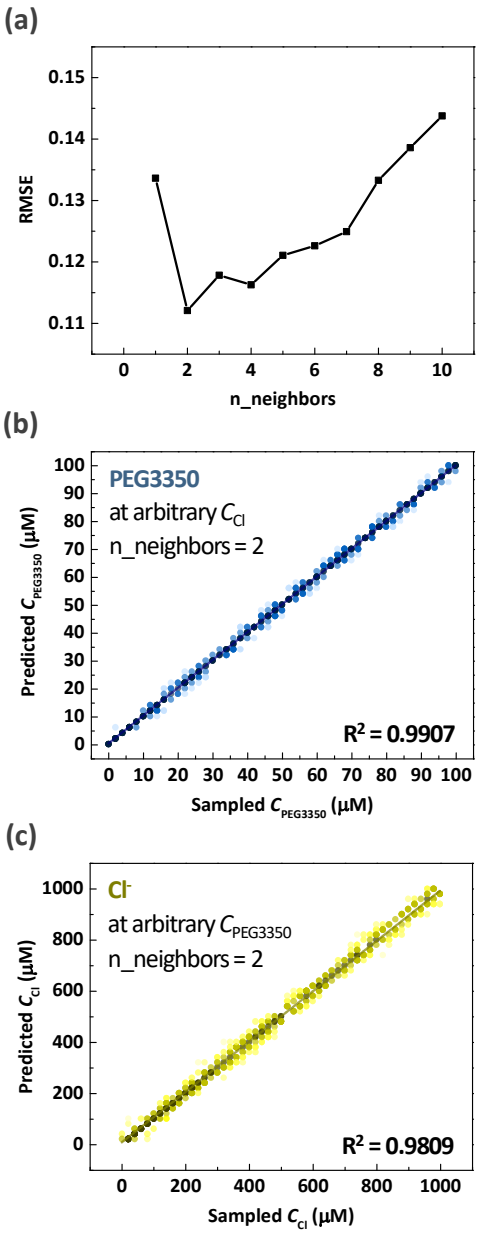

Figure 3.20. (a) RMSE with various n_neighbors values, and the performance of concentration prediction for (b) PEG3350 and (c) Cl^- in VMS using k-NN.

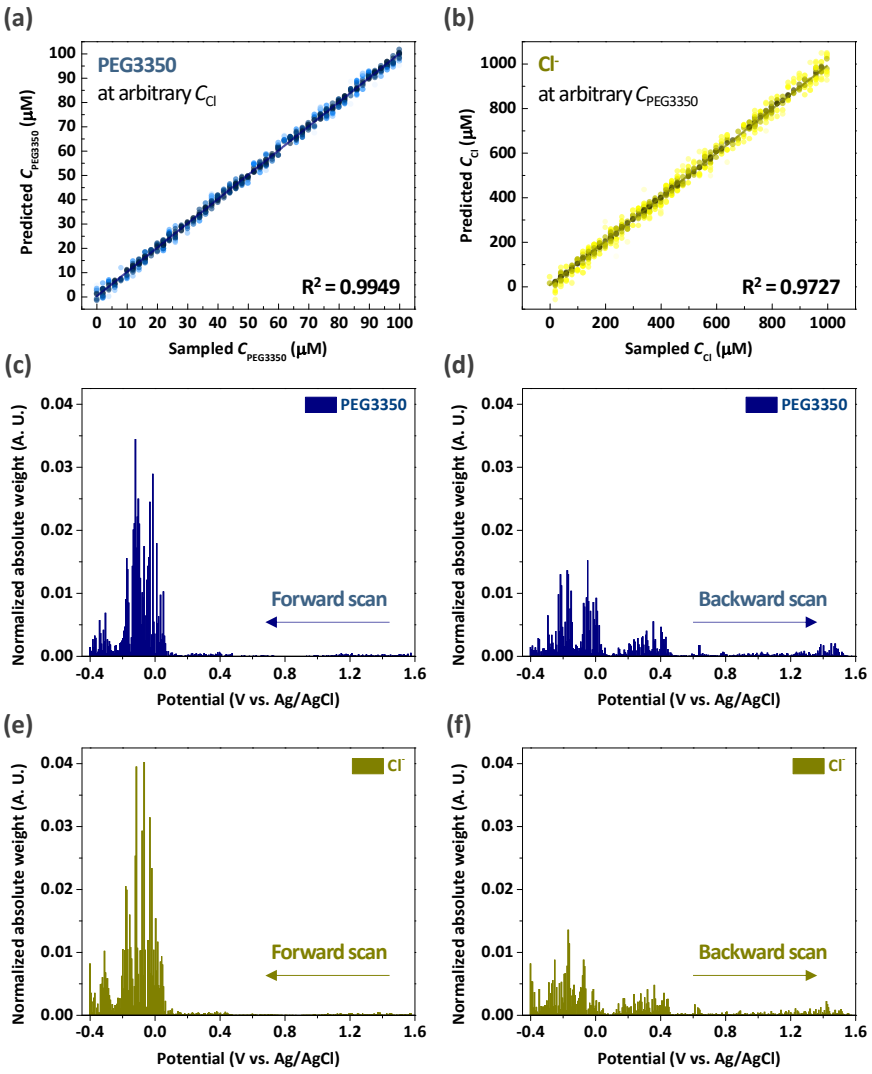

Figure 3.21. The performance of concentration prediction for (a) PEG3350 and (b) Cl^-, and normalized absolute weight of (c) forward scan and (d) backward scan for PEG3350, and (e) forward scan and (f) backward scan for Cl^- in VMS using linear model.

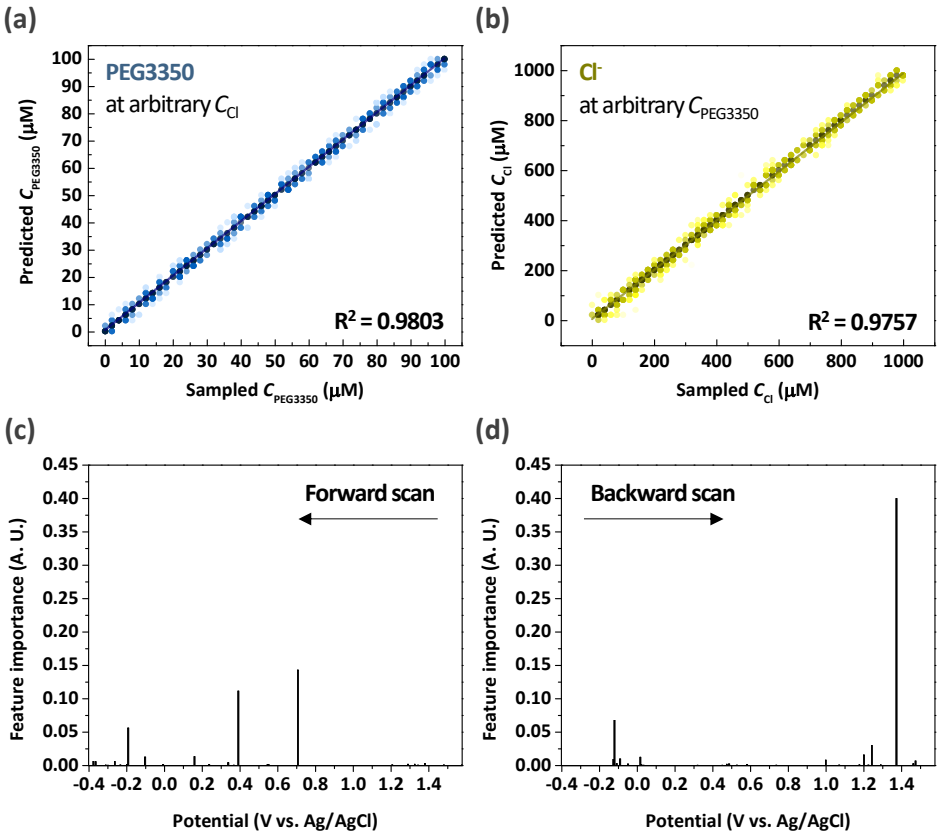

Figure 3.22. The performance of concentration prediction for (a) PEG3350 and (b) Cl^-, and feature importance of (c) forward scan and (d) backward scan using decision tree.

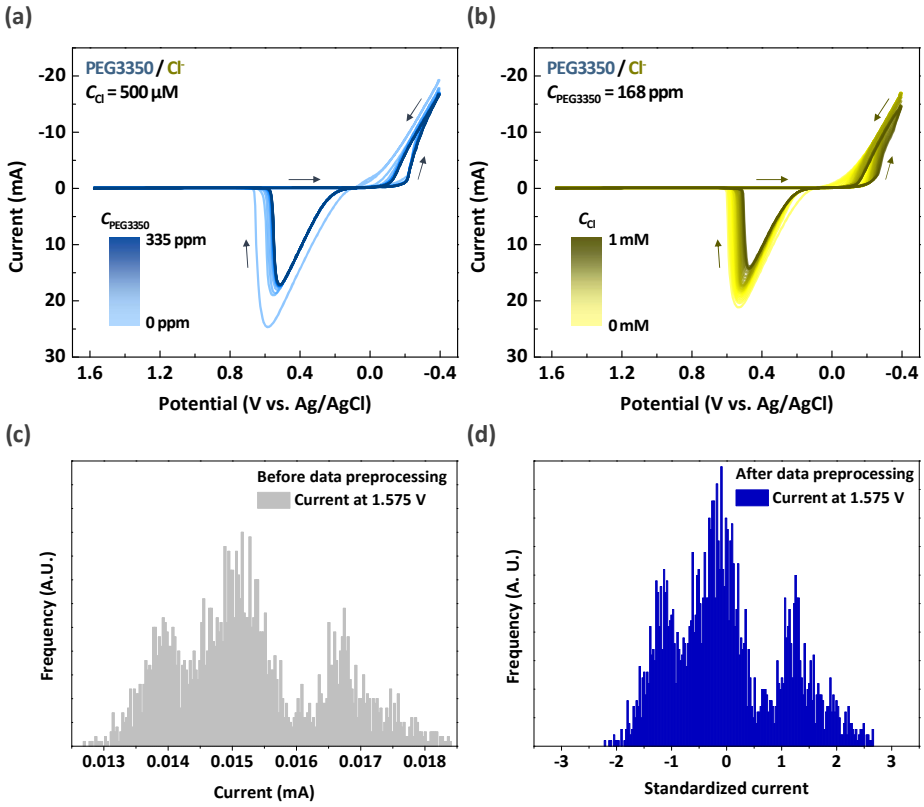

Figure 3.23. CV analysis with various concentrations of (a) PEG3350 and (b) Cl^- in VMS, and current distribution (c) before and (d) after data preprocessing.

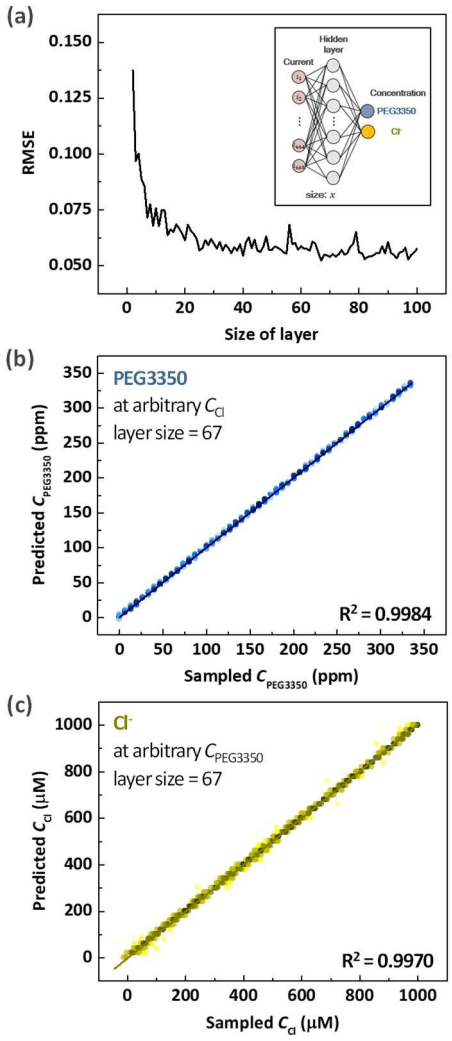

Figure 3.24. (a) Root mean square error (RMSE) with various layer sizes and the performance of concentration prediction for (b) PEG3350 and (c) Cl^- in VMS.

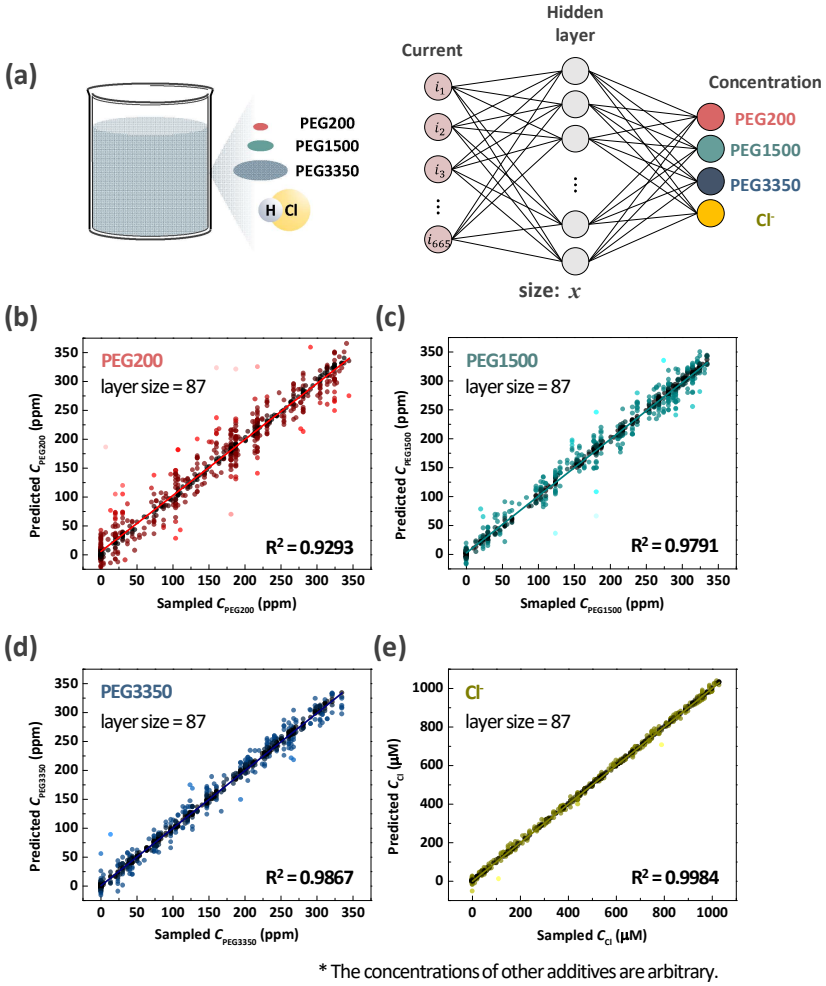

Figure 3.25. (a) Additive system in Cu electrodeposition and neural network model, and performance of predicting (b) PEG200, (c) PEG1500, (d) PEG3350, and (e) Cl^- concentration in VMS. The concentrations of PEG200, PEG1500, PEG3350 and Cl^- are randomly selected.

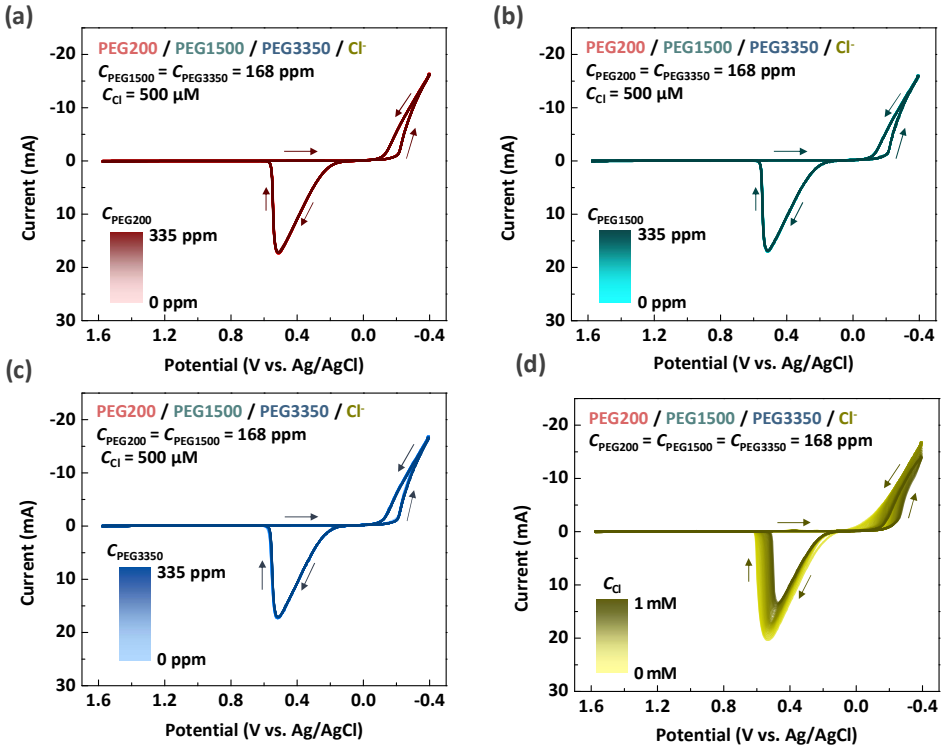

Figure 3.26. CV analysis with various concentrations of (a) PEG200, (b) PEG1500, (c) PEG3350, and (b) Cl^- in VMS.

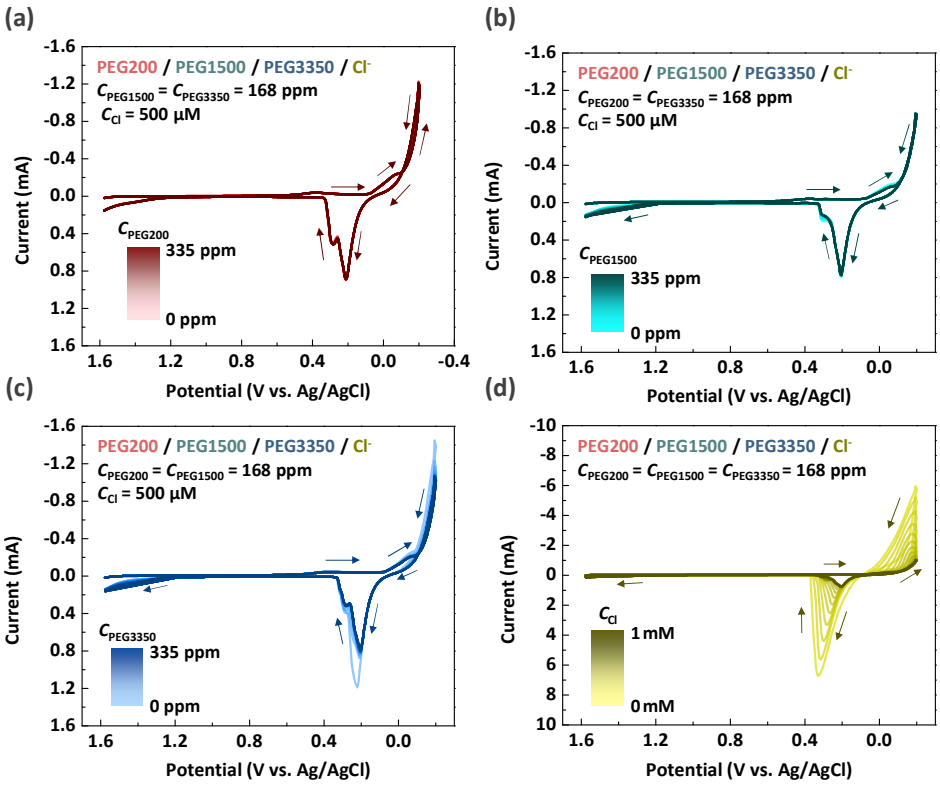

Figure 3.27. CV analysis with various concentrations of (a) PEG200, (b) PEG1500, (c) PEG3350, and (b) Cl^- in VMS after change in the vertex potential from –0.4 $V_{Ag/AgCl}$ to –0.2 $V_{Ag/AgCl}$.

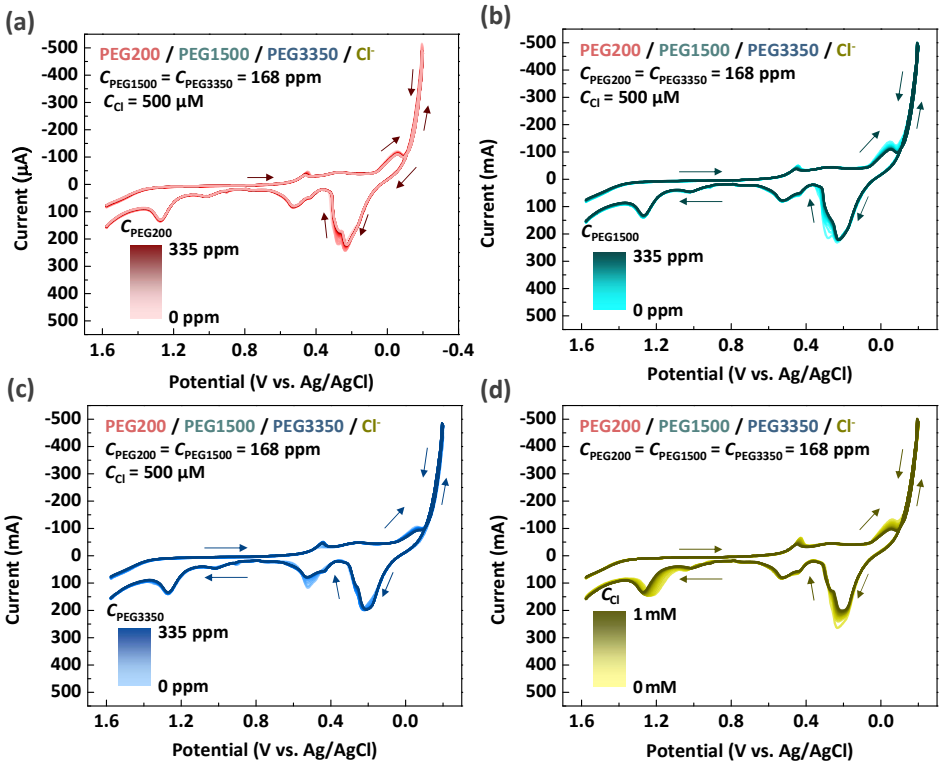

Figure 3.28. CV analysis with various concentrations of (a) PEG200, (b) PEG1500, (c) PEG3350, and (b) Cl^- in VMS after change in the vertex potential from –0.4 $V_{Ag/AgCl}$ to –0.2 $V_{Ag/AgCl}$ and adding 500 µM NH_4I into the base solution.

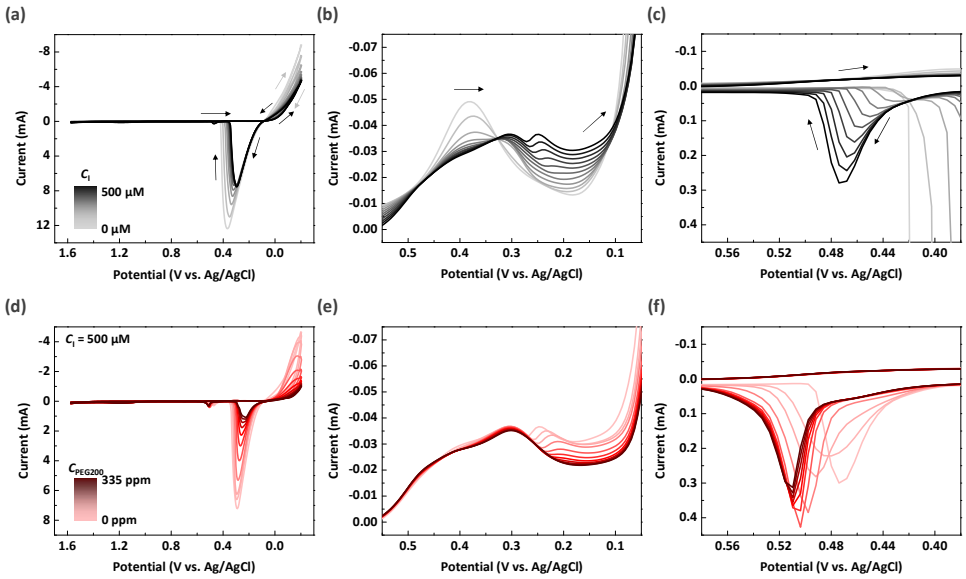

Figure 3.29. CV analysis with various concentrations of (a) I^- in VMS, and its enlarged figure at (b) 0.45 V to 0.05 V and (c) 0.58 V to 0.38 V. CV analysis with various concentrations of (d) PEG200 in VMS after the addition of I^-, and its enlarged figure at (e) 0.45 V to 0.05 V and (f) 0.58 V to 0.38 V.

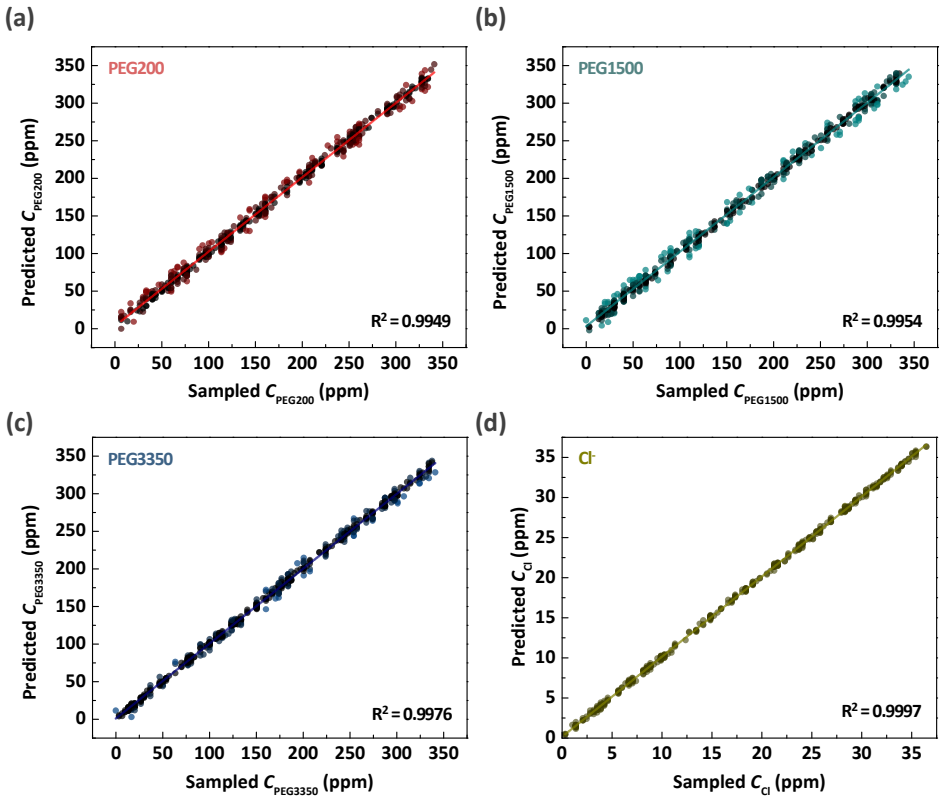

Figure 3.30. Performance of predicting (a) PEG200, (b) PEG1500, (c) PEG3350, and (d) Cl^- concentration in in VMS using I^- pretreatment. The concentrations of PEG200, PEG1500, PEG3350 and Cl^- are randomly selected.

CHAPTER IV

Conclusion

The concentration of I^- in the TSV filling solution was the most influential factor affecting the TSV filling performance. An excellent filling performance by 400 μM of I^- was shown, while voids were formed when C_I was less than 300 μM. CuI and I_2, the major predicted by-product from I^-, seemed to have a negligible effect. In order to monitor the C_I in a three-additive acidic plating solution, RC-CVS analysis was conducted. I^- showed a convection-dependent inhibition and the high rotating speed thus led to a fast $Q/\underline{Q}_0$ drop. The inhibition of I^- drastically decreased when the vertex potential was set to a more negative value than –0.2 V due to the reduction of CuI, which was further confirmed in effective coverage analysis. Based on the optimum condition with a higher effective coverage, C_I was successfully determined in various Cu acidic plating solutions. This CVS analysis was applied to monitor the Cu plating solution for the TSV filling. During the degradation, 145 μM of I^- was consumed and the concentration was determined. After the addition of I^-, void-free filling was obtained, which suggests that the CVS analysis can be used for monitoring the TSV filling performance.

In the two-additive Cu plating solution, SPS, the accelerator, affected the determination of C_S in target solutions, when using conventional DT-CVS analysis. Even in low C_A, the determined C_S was distorted with errors up to 19 μM, because the EPE-Cu^+-Cl^- layer is easily destroyed by SPS. In order to prevent the interference of SPS in the C_S determination in two-additive Cu plating solution, I^- was chosen, based on the acting mechanism of halide in Cu electrodeposition. The 400 μM of I^- prevented the anti-suppression action of SPS (C_A = 10 μM) to an extent in Cu electroplating at C_S = 2 μM, and this exclusion of interference was perfectly achieved at negative vertex potential and slow scan rate. The low solubility of CuI due to high polarizability of I^- and hydrophobic characteristic formed a much more stable and sufficient EPE-Cu^+-I^- layer in slower electrochemical sweeping, stopping the passivation layer from the breakdown by SPS. Even CuI alone effectively inhibits the adsorption of SPS on the electrode surface. The synergistic interaction between CuI and EPE supported the re-formation of the passivation layer after the disruption by the inner diffusion of Cu^{2+}/Cu^+ ions in reverse sweep. Under the pre-optimized condition, modified CVS analysis was performed, and the Q/Q_0 plots showed the same response to C_S in the CVS bath, irrespective of the C_A in solutions. The different C_S values in various target solutions

were determined, and the results exhibited high linearity with wide range of (10 to 70) μM.

In the case of species which do not directly participate in the electrochemical reaction, quantitative analysis of the species is performed based on its effect on the specific electrochemical reaction, instead of observing the current peak of an electrochemical reaction occurs in CV analysis. The problem with this approach is that it requires chemical/electrochemical conditions to selectively determine only the concentration of the species. Concentration analysis model using machine learning has an advantage in that this method could be approached without understanding about these conditions. In a system with a simple chemical composition composed of PEG3350 and Cl^-, a neural network model could be implemented which could predict the concentration of each component without any special chemical pretreatment. In a system with a complex chemical composition consisting of PEG3350/PEG1500/PEG200/Cl^-, the lower the molecular weight of PEG, the worse the performance in predicting concentration due to the competition in adsorption between PEGs caused by the limited amount of Cl^- and low CV responsiveness of the low molecular weight PEG. In order to enhance the CV responsiveness of each PEG, the switching potential was shifted from –0.4 $V_{Ag/AgCl}$ to –0.2 $V_{Ag/AgCl}$, and as a result of the pretreatment with I^- in the basis analyte, the CV

responsiveness of PEG200 was improved, resulting in the implementation of a neural network model capable of predicting the concentration of all PEGs and Cl^-. Consequently, when the understanding of the Cu electrochemical deposition system and machine learning are combined, it is possible to build a model capable of prediction the additive concentration using electrochemical analysis even in complex additive compositions.

References

[1] R. R. Tummala, et al., *Ieee Transactions on Advanced Packaging*, **27**, 250 (2004).

[2] J. H. Lau, *Microelectron. Int.*, **28**, 8 (2011).

[3] M. Motoyoshi, *Proc. IEEE*, **97**, 43 (2009).

[4] D. Josell and T. P. Moffat, *J. Electrochem. Soc.*, **165**, D23 (2018).

[5] T. P. Moffat and D. Josell, *J. Electrochem. Soc.*, **159**, D208 (2012).

[6] D. Josell and T. P. Moffat, *J. Electrochem. Soc.*, **162**, D129 (2015).

[7] T. M. Braun, et al., *J. Electrochem. Soc.*, **165**, D291 (2018).

[8] D. Josell and T. P. Moffat, *J. Electrochem. Soc.*, **163**, D322 (2016).

[9] D. Josell, et al., *J. Electrochem. Soc.*, **163**, D809 (2016).

[10] D. Josell and T. P. Moffat, *J. Electrochem. Soc.*, **164**, D327 (2017).

[11] D. Roha and U. Landau, *J. Electrochem. Soc.*, **137**, 824 (1990).

[12] M. J. Kim, et al., *J. Electrochem. Soc.*, **163**, D434 (2016).

[13] M. J. Kim, et al., *Electrochim. Acta*, **163**, 174 (2015).

[14] M. J. Kim, et al., *J. Electrochem. Soc.*, **163**, D185 (2016).

[15] W. P. Dow, et al., *J. Electrochem. Soc.*, **152**, C425 (2005).

[16] S. M. Huang, et al., *J. Electrochem. Soc.*, **159**, D135 (2012).

[17] M. H. Lee, et al., *J. Electrochem. Soc.*, **164**, D1051 (2017).

[18] M. J. Kim, et al., *J. Electrochem. Soc.*, **160**, D3081 (2013).

[19] M. J. Kim, et al., *J. Electrochem. Soc.*, **160**, D3088 (2013).

[20] W. P. Dow, et al., *Electrochemical and Solid State Letters*, **9**, C134 (2006).

[21] A. Lee, et al., *Korean J. Chem. Eng.*, **36**, 981 (2019).

[22] P. M. Vereecken, et al., *Ibm Journal of Research and Development*, **49**, 3 (2005).

[23] W. P. Dow, et al., *J. Electrochem. Soc.*, **152**, C769 (2005).

[24] Z. V. Feng, et al., *J. Phys. Chem. B*, **107**, 9415 (2003).

[25] J. P. Healy, et al., *J. Electroanal. Chem.*, **338**, 155 (1992).

[26] D. Stoychev, *Trans. Inst. Met. Finish.*, **76**, 73 (1998).

[27] D. Stoychev and C. Tsvetanov, *J. Appl. Electrochem.*, **26**, 741 (1996).

[28] J. W. Gallaway and A. C. West, *J. Electrochem. Soc.*, **155**, D632 (2008).

[29] J. W. Gallaway, et al., *J. Electrochem. Soc.*, **156**, D287 (2009).

[30] K. Ryan, et al., *J. Electrochem. Soc.*, **160**, D3186 (2013).

[31] N. Xiao, et al., *Electrochim. Acta*, **116**, 284 (2014).

[32] W. P. Dow and H. S. Huang, *J. Electrochem. Soc.*, **152**, C67 (2005).

[33] W. P. Dow, et al., *J. Electrochem. Soc.*, **152**, C77 (2005).

[34] B. Bozzini, et al., *J. Electrochem. Soc.*, **153**, C254 (2006).

[35] T. P. Moffat, et al., *J. Electrochem. Soc.*, **151**, C262 (2004).

[36] M. J. Willey and A. C. West, *J. Electrochem. Soc.*, **154**, D156 (2007).

[37] M. Tan, et al., *J. Electrochem. Soc.*, **154**, D78 (2007).

[38] M. L. Walker, et al., *J. Electrochem. Soc.*, **153**, C557 (2006).

[39] T. P. Moffat, et al., *J. Electrochem. Soc.*, **147**, 4524 (2000).

[40] T. P. Moffat, et al., *Ibm Journal of Research and Development*, **49**, 19 (2005).

[41] T. P. Moffat, et al., *J. Electrochem. Soc.*, **153**, C127 (2006).

[42] T. P. Moffat, et al., *Electrochim. Acta*, **53**, 145 (2007).

[43] M. A. Pasquale, et al., *Electrochim. Acta*, **53**, 5891 (2008).

[44] N. T. M. Hai and P. Broekmann, *Chemelectrochem*, **2**, 1096 (2015).

[45] V. Q. Dinh, et al., *J. Electrochem. Soc.*, **167**, 7 (2020).

[46] M. Sung, et al., *J. Electrochem. Soc.*, **166**, D546 (2019).

[47] M. Hayase and M. Nagao, *J. Electrochem. Soc.*, **160**, D3216 (2013).

[48] H. C. Kim, et al., *J. Electrochem. Soc.*, **165**, D91 (2018).

[49] M. Tomie, et al., *J. Electrochem. Soc.*, **167** (2020).

[50] V. Q. Dinh, et al., *J. Electrochem. Soc.*, **166**, D505 (2019).

[51] W. P. Dow, et al., *Electrochim. Acta*, **53**, 8228 (2008).

[52] M. H. Lee, et al., *J. Electrochem. Soc.*, **167**, 102505 (2020).

[53] W. P. Dow, et al., *J. Electrochem. Soc.*, **156**, D314 (2009).

[54] M. X. Tang, et al., *Rsc Advances*, **7**, 40342 (2017).

[55] S. J. Ren, et al., *J. Electrochem. Soc.*, **162**, D509 (2015).

[56] L. Zheng, et al., *Electrochim. Acta*, **283**, 560 (2018).

[57] J. Li, et al., *Acs Omega*, **5**, 4868 (2020).

[58] X. M. Wang, et al., *Dyes Pigm.*, **181**, 108594 (2020).

[59] B. Bozzini, et al., *Electrochim. Acta*, **52**, 4767 (2007).

[60] J. J. Kelly, et al., *J. Electrochem. Soc.*, **146**, 2540 (1999).

[61] M. J. Willey, et al., *Electrochemical and Solid State Letters*, **10**, D38 (2007).

[62] N. T. M. Hai, et al., *J. Electrochem. Soc.*, **160**, D3116 (2013).

[63] C. Gabrielli, et al., *J. Appl. Electrochem.*, **38**, 457 (2008).

[64] C. Gabrielli, et al., *J. Electrochem. Soc.*, **154**, D163 (2007).

[65] S. Choe, et al., *J. Electrochem. Soc.*, **160**, D3179 (2013).

[66] T. Y. Kim, et al., *J. Electrochem. Soc.*, **166**, G61 (2019).

[67] Y. S. Won, et al., *J. Appl. Polym. Sci.*, **117**, 2083 (2010).

[68] S. Choe, et al., *J. Electroanal. Chem.*, **714**, 85 (2014).

[69] T. Y. Kim, et al., *Electrochim. Acta*, **357** (2020).

[70] S. Choe, et al., *J. Electrochem. Soc.*, **163**, D33 (2016).

[71] S. Choe, et al., *J. Electrochem. Soc.*, **162**, H294 (2015).

[72] S. Choe, et al., *J. Electrochem. Soc.*, **163**, D747 (2016).

[73] Y. LeCun, et al., *Nature*, **521**, 436 (2015).

[74] J. Schmidhuber, *Neural Networks*, **61**, 85 (2015).

[75] T. G. Dietterich, in *Multiple Classifier Systems*, J. Kittler and F. Roli Editors, p. 1 (2000).

[76] L. Breiman, *Machine Learning*, **45**, 5 (2001).

[77] C. Cortes and V. Vapnik, *Machine Learning*, **20**, 273 (1995).

[78] K. T. Butler, et al., *Nature*, **559**, 547 (2018).

[79] F. Pedregosa, et al., *Journal of Machine Learning Research*, **12**, 2825 (2011).

[80] D. A. Palmer, et al., *J. Solution Chem.*, **13**, 673 (1984).

[81] T. M. T. Huynh, et al., *Electrochim. Acta*, **89**, 537 (2013).

국문 초록

구리 전해 도금조의 화학적 조성을 정확하게 모니터링하는 것은 장기적이고 반복적인 도금 작업 중에 도금조의 성능을 유지하기 위한 핵심 요소이다. 구리 전해 도금 공정에서 첨가제의 농도를 모니터링하는 것이 중요해지고 있지만 첨가제 간의 상호 작용으로 인해 대상 첨가제의 독립적인 거동을 관찰하기 어렵기 때문에 이는 매우 도전적이다. 첨가제에 대한 모니터링은 일반적으로 전기화학 분석으로 진행된다. 전기화학 분석은 경제적이고 접근성이 빠르며 한 번에 많은 정보를 취합할 수 있다는 장점이 있으며 구리 전해 도금 시스템의 첨가제와 같이 전기화학 반응에 직접 참여하지 않는 화학종의 경우, 분석 신호로부터 직접적으로 양적인 정보를 얻기가 어렵지만 첨가제의 농도에 따라 달라지는 구리 이온의 전기화학 환원 속도를 통해 간접적으로 그 양적 정보를 추측할 수 있다. 기존의 이러한 방식은 전기화학 반응에 직접적으로 참여하지 않는 화학종에 대해서도 그 양적 정보에 대한 추정이 가능하다는 장점이 있지만, 구리 전해 도금 시스템이 많은 첨가제를 포함하는 경우, 각 첨가제들이 구리 이온의 환원 속도에 복합적으로 영향을 미치므로 전기화학 분석에서 발생하는 신호가 어떤 첨가제로 인한 것인지를 파악하기가 어렵다.

본 연구에서는 화학적 제어와 전기화학적 제어를 통해 표적 첨가제의 선택도를 높이는 전기화학 측정 방법에 대해서 다룬다. 무기 평탄제인 요오드화 이온(I^-)은 유기물과 같이 전혀 다른 성질의 분해 산물을 만들지 않는다는 점에서 우수한 첨가제로 평가받고 있다. 구리 전해 도금 과정에서 요오드화 이온은 구리 1 가 이온(Cu^+)과의 반응과 산화 반응 및 물리적 함입에 의해 소모되었다. 요오드화 이온의 감소는 도금조의 성능 저하를 가져오는 반면 주요 부산물인 요오드(I_2)와 요오드화 구리(CuI)는 도금조의 실리콘 관통 전극(through-silicon via, TSV) 충진 성능에 거의 영향을 미치지 않았다. Cyclic voltammetry stripping (CVS) 분석을 통해 요오드화 농도를 모니터링하기 위해 요오드화 이온의 전기화학적 반응을 다양한 조건에서 조사하였으며 이를 통해 요오드화 이온이 구리 전해 도금 속도를 억제하는 정도가 요오드화 이온의 물질 전달과 음극 전위에 따라 달라진다는 것을 확인하였다. 이후의 effective coverage 분석은 요오드화 이온뿐만 아니라 CuI 가 주요 억제제로 작용하며, 요오드화 이온의 억제가 음의 포텐셜에서 약해짐을 보여준다. 최적화된 조건에서 수행된 반응 곡선 분석을 통해 다른 첨가제의 농도에 관계없이 실제 농도와 측정된 농도 사이의 선형 관계를 얻을 수 있었으며, 이는 구리 전해 도금조에서 요오드화 농도를 직접 모니터링할 수 있게 하였다.

Bis-(3-sulfopropyl)-disulfide (SPS)는 구리 전해 도금에서 사용되는 대표적인 가속제로 polyalkyl glycol (PAG)의 억제 작용을 방해하며, 따라서 SPS 의

존재는 PAG 농도 측정에 있어서 signal-to-noise ratio (SNR)를 낮추는 문제를 일으킨다. SPS 의 억제 방해 작용을 줄이면서 PAG 농도를 측정하기 위해 격렬한 물질 전달 환경에서 가속제의 작용을 저해할 수 있는 요오드화 이온을 전처리제로 도입하였다. CVS 방법을 모니터링 도구로 사용할 때 표적 용액 내 극소량의 SPS 도 PAG 농도 측정에 상당히 큰 오차를 유발하였다. 요오드화 이온은 SPS 의 농도에 관계없이, SPS 가 매개하는 표면 passivation 층의 파괴를 저해하여 SPS 의 간섭 없이 PAG 농도를 선택적으로 결정할 수 있게 했다. 이는 다양한 전기화학 분석 및 표면 분석을 통해 전극 표면에서 CuI 가 형성되면서 PAG 와 복합체를 형성하고 이를 통해 형성되는 억제 층이 기존의 염화 이온(Cl^-)과 함께 만들어지는 억제 층에 비해 강하기 때문인 것으로 추정되었다. 요오드화 이온을 도입함으로써 수정된 CVS 분석이 제안되었고, 결과적으로 요오드화 이온을 첨가하면 분석액 내 SPS 의 농도에 관계없이 실제 값과 유사하게 결정된 PAG 농도를 산출할 수 있었다.

머신 러닝은 데이터에서부터 컴퓨터 스스로가 학습하도록 프로그래밍하는 기술로 통계적 모델을 많은 양의 데이터와 컴퓨터의 연산 능력을 통해 최적화하여 시스템에 대한 예측을 가능하게 한다. 머신 러닝은 어떻게 작동되는지 아직 정확히 밝혀지지 않은 시스템의 문제를 시스템 자체의 작동 메커니즘을 파악하는 것이 아닌, 시스템으로부터 만들어지는 데이터를 통해 해결할 수 있으며 시스템에 변화가 발생해도 이를 학습하여 이러한

변화에 스스로 적응이 가능하다는 장점이 있다. 전기화학 분석의 장점과 머신 러닝을 결합할 때 시스템 변수에 대한 전기화학 데이터 학습을 통해 유의미한 정보를 추출할 수 있는 모델 및 학습된 모델을 통해 전기화학 시스템의 작동 메커니즘에 대한 이해를 높일 수 있다는 기대를 할 수 있다. Cl^-는 구리 전해 도금 과정에서 기판 표면에 먼저 흡착하여 polyethylene glycol (PEG)의 강한 흡착을 유도하는 견인 역할을 하며 PEG 와 Cl^-의 상호작용으로 인해 구리 이온의 환원에 필요한 에너지를 증가시켜 그 속도를 늦추며 둘의 상호 보완적인 효과로 인해 각각의 농도를 선택적으로 측정하는 것은 매우 어렵다. PEG3350 과 Cl^-로 구성된 시스템에서는 단순한 전기화학 분석을 통해 수집된 데이터와 인공 신경망 모델을 통해서도 쉽게 농도 측정이 가능했으며 이는 PEG3350 과 Cl^-의 뛰어난 cyclic voltammetry (CV) 응답성으로 인한 것이다. 하지만 PEG200, PEG1500, PEG3350 과 Cl^-와 같이 다양한 분자량의 PEG 를 포함한 구리 전해 도금 시스템에서는 같은 전기화학 분석과 모델을 적용했을 때 농도 예측 성능이 떨어졌다. 이는 Cl^-가 전극 표면에 PEG 를 위한 흡착 점으로 작용하는 상황에서 제한된 수의 Cl^-를 두고 PEG 사이에서 흡착 경쟁이 발생하기 때문이며, 특히 PEG200 의 경우 분자량이 작아 구리 전해 도금에 영향을 미치지 못하기 때문에 농도 예측의 성능이 떨어졌다. PEG 의 흡착을 제어하기 위해 CV 분석의 vertex 전위를 –0.4 V 에서 –0.2 V 로 변환하였으며 요오드화 이온 전처리를 통해 PEG200 의 CV 응답성을 획기적으로 증대시켰다. 이는 요오드화 이온의

도입이 구리 전해 도금 이외에 구리 이온의 환원과 그 과정에서 형성되는 CuI 의 산화와 같이 다양한 구리-요오드 전기화학 반응계를 만들어내며 이 복잡한 반응에 PEG 가 분자량별로 서로 다른 영향을 미치기 때문인 것으로 추정된다. 결과적으로 전기화학적 제어와 요오드화 이온 화학적 전처리를 도입하여 PEG 와 Cl^-의 농도 분석에 대한 SNR 을 획기적으로 줄였으며 인공 신경망 모델의 성능을 향상시킬 수 있었다.

주요어: 구리 전해 도금, 첨가제, 선택적 모니터링, 전기화학 분석, 머신 러닝

학번: 2016-21041